AGU PUBLICATIONS

JGR

Journal of Geophysical Research: Atmospheres

RESEARCH ARTICLE
10.1002/2016JD026125

Key Points:
- Crop albedo enhancement and irrigation are more effective at reducing hot temperature extremes than mean temperature
- Using irrigation with crop albedo enhancement produces the most robust cooling response
- Regional differences exist and are a function of changes in the surface energy balance triggered by climate-effective land management

Supporting Information:
- Supporting Information S1

Correspondence to:
A. L. Hirsch and S. I. Seneviratne,
annette.hirsch@env.ethz.ch;
sonia.seneviratne@ethz.ch

Citation:
Hirsch, A. L., M. Wilhelm, E. L. Davin, W. Thiery, and S. I. Seneviratne (2017), Can climate-effective land management reduce regional warming?, *J. Geophys. Res. Atmos.*, *122*, 2269–2288, doi:10.1002/2016JD026125.

Received 21 OCT 2016
Accepted 11 FEB 2017
Accepted article online 14 FEB 2017
Published online 28 FEB 2017

Can climate-effective land management reduce regional warming?

A. L. Hirsch[1], M. Wilhelm[1], E. L. Davin[1], W. Thiery[1,2], and S. I. Seneviratne[1]

[1]Institute for Atmospheric and Climate Science, ETH Zurich, Zurich, Switzerland, [2]Department of Hydrology and Hydraulic Engineering, Vrije Universiteit Brussel, Brussels, Belgium

Abstract Limiting global warming to well below 2°C is an imminent challenge for humanity. However, even if this global target can be met, some regions are still likely to experience substantial warming relative to others. Using idealized global climate simulations, we examine the potential of land management options in affecting regional climate, with a focus on crop albedo enhancement and irrigation (climate-effective land management). The implementation is performed over all crop regions globally to provide an upper bound. We find that the implementation of both crop albedo enhancement and irrigation can reduce hot temperature extremes by more than 2°C in North America, Eurasia, and India over the 21st century relative to a scenario without management application. The efficacy of crop albedo enhancement scales with the magnitude, where a cooling response exceeding 0.5°C for hot temperature extremes was achieved with a large (i.e., ≥0.08) change in crop albedo. Regional differences were attributed to the surface energy balance response with temperature changes mostly explained by latent heat flux changes for irrigation and net shortwave radiation changes for crop albedo enhancement. However, limitations do exist, where we identify warming over the winter months when climate-effective land management is temporarily suspended. This was associated with persistent cloud cover that enhances longwave warming. It cannot be confirmed if the magnitude of this feedback is reproducible in other climate models. Our results overall demonstrate that regional warming of hot extremes in our climate model can be partially mitigated when using an idealized treatment of climate-effective land management.

1. Introduction

Recent research illustrates that as a consequence of global anthropogenic climate change, some regions will warm at an accelerated rate relative to the global mean temperature anomaly [*Seneviratne et al.*, 2016]. Despite the recent global commitment to limit global warming to well below 2°C [*United Nations Framework Convention on Climate Change*, 2015] and to reduce greenhouse gas (GHG) emissions accordingly, some regions will still experience a substantially higher magnitude of warming even for this agreed global warming target [*Seneviratne et al.*, 2016]. Consequently, this has severe implications on the ability of these regions to adapt to climate change.

Climate engineering has been in the research discourse for more than 50 years (see reviews from *Keith* [2000], *Crutzen* [2006], *Wigley* [2006], and *Caldeira and Bala* [2016]) and is considered by some as a possible means to achieve this 2°C limit [e.g., *Keith and Irvine*, 2016]. Climate engineering involves the deliberate modification of the Earth's climate system to counteract anthropogenic climate change [*Intergovernmental Panel on Climate Change (IPCC)*, 2013] and can be split between two paradigms: those that involve carbon dioxide removal or changes in the Earth's radiation balance. Most carbon dioxide removal concepts are also associated with conventional mitigation activities that can involve carbon sequestration from reforestation and afforestation [e.g., *Sonntag et al.*, 2016]. Proposed schemes altering the radiation balance include, solar reduction geoengineering [*Irvine et al.*, 2010; *Schaller et al.*, 2014; *Cao et al.*, 2016], stratospheric aerosol injection [*Robock et al.*, 2008; *Jones et al.*, 2010; *Tjiputra et al.*, 2016], marine cloud brightening [*Jones et al.*, 2009; *Muri et al.*, 2015], cirrus cloud thinning [*Kristjansson et al.*, 2015], desert albedo modification [*Irvine et al.*, 2011; *Crook et al.*, 2015], ocean albedo modification [*Crook et al.*, 2016; *Gabriel et al.*, 2017], and crop albedo modification [*Singarayer et al.*, 2009; *Davin et al.*, 2014; *Wilhelm et al.*, 2015]. Using idealized simulations with Earth System Models (ESMs), the Geoengineering Model Intercomparison Project (GeoMIP) [*Kravitz et al.*, 2011, 2013a, 2013b, 2015] examines the efficacy of various climate engineering schemes to negate warming induced by higher GHG concentrations. For example, the GeoMIP G1 experiment [*Kravitz et al.*, 2011] illustrated that climate engineering via solar reduction geoengineering can reverse the warming associated

with a quadrupling of carbon dioxide concentration; however, the corresponding response of the hydrological cycle suggests possible negative consequences for several regions [*Kravitz et al*., 2013b; *Tilmes et al*., 2013].

Comparisons across different climate engineering schemes are few [e.g., *Lenton and Vaughan*, 2009; *Vaughan and Lenton*, 2011; *Irvine et al*., 2011; *Niemeier et al*., 2013; *Crook et al*., 2015; *Irvine et al*., 2016]. However, *Crook et al*. [2015] examined the surface temperature and precipitation response of six climate engineering schemes using single realizations from an ESM. They found that solar reduction geoengineering, marine cloud brightening, cirrus cloud thinning, and ocean albedo modification were the most effective at inducing global cooling of the planet of the order of 1°C. Desert albedo modification was found to induce substantial changes in global circulation and the hydrological cycle, similar to results reported by *Irvine et al*. [2011]. *Crook et al*. [2015] also examined the potential of crop albedo enhancement but found the effect on mean temperature to be negligible relative to the other climate engineering schemes that they evaluated. They also identify a rapid warming at the termination of all climate engineering schemes except for crop albedo enhancement, as it has no strong cooling effect globally. This imposes an ethical constraint on climate engineering, where the commencement of most schemes requires the long-term commitment of future generations to the continuation of climate engineering to avoid the consequences of sudden termination [e.g., *Jones et al*., 2013]. This is particularly true if one adopts an "all or nothing" approach to climate engineering [*Keith and Irvine*, 2016]. Despite the comparatively limited efficacy of crop albedo enhancement in contrast to other climate engineering schemes reported in the literature, it has some advantages. This includes using existing agricultural management techniques and therefore can be considered as a supplement to existing land management practice.

Climate-effective land management (CeLM) considers more than just crop albedo enhancement and can involve a diverse range of existing land management practices including double cropping, crop dusting, conservation tillage, forest management, and irrigation [*Lobell et al*., 2006; *Wilhelm et al*., 2015]. Most of these practices are currently used in agricultural landscapes, with almost two thirds of the global land surface already under a substantial level of management [*Luyssaert et al*., 2014].

The impact of various land management practices on surface climate has been examined before [e.g., *Lobell et al*., 2006; *Ridgwell et al*., 2009; *Doughty et al*., 2011; *Irvine et al*., 2011; *Davin et al*., 2014; *Wilhelm et al*., 2015]. Using idealized ESM simulations, *Lobell et al*. [2006] examine the mean temperature response to irrigation, no-till management, second-growing season, and double cropping under present-day GHG concentrations. All schemes were found to have a regional cooling effect, with irrigation having the largest global cooling effect on mean temperature of 1.3°C over land. *Ridgwell et al*. [2009] extended this to consider the efficacy of different levels of crop albedo enhancement under elevated CO_2 concentrations. They also find that increasing crop albedo can lead to more than 1°C cooling of mean summertime temperatures over agricultural landscapes. However, both studies focus on the potential of CeLM schemes to cool mean temperature with no examination of what this means for extreme temperatures.

Using a regional climate model to simulate present-day climate, *Davin et al*. [2014] examine the potential of no tillage to cool surface climate over Europe. They find an amplified cooling effect on temperature extremes relative to means. This approach was extended by *Wilhelm et al*. [2015] to consider albedo enhancement over all vegetation types to mitigate temperature extremes for present and future climate. They find that decreases in daily maximum temperature (T_{MAX}) scale linearly with the magnitude of albedo enhancement with strong preferential cooling of hot extremes over the northern midlatitudes during boreal summer (June–August: JJA). *Wilhelm et al*. [2015] also show that the spatial extent of albedo enhancement is critical for the magnitude of cooling at the global scale. In particular, reducing the spatial extent of albedo enhancement to agricultural regions and the temporal extent to boreal summer showed smaller changes in T_{MAX}.

In this paper we use idealized ESM simulations to examine the efficacy of CeLM to reduce regional warming of hot extremes associated with future anthropogenic climate change. By considering the impact of different CeLM schemes on projected changes in temperature extremes with anthropogenic climate change, we differentiate our research from that of *Lobell et al*. [2006] and *Ridgwell et al*. [2009]. We extend the approach of *Davin et al*. [2014] and *Wilhelm et al*. [2015] to compare the efficacy of crop albedo enhancement, irrigation, and the application of both schemes. To our knowledge we are the first study to examine the combined effect of crop albedo enhancement and irrigation. We note that the experiments are idealized and that they are a global implementation of crop albedo enhancement and irrigation. In reality, such modifications are

more likely to occur at a regional scale, and therefore, our experiment provides an upper bound on what is possible with CeLM. Finally, we aim to identify regions where particular CeLM schemes are more effective and determine whether differences in regional responses are associated with how CeLM affects the surface energy balance.

2. Methods

2.1. Model Description

We use the Community Earth System Model version 1.2 [*Hurrell et al*., 2013], a state-of-the-art climate model that consists of component models representing the atmosphere, land, ocean, sea ice, land ice, and their interactions. This climate model has been extensively evaluated [e.g., *Gent et al*., 2011; *Hurrell et al*., 2013; *Meehl et al*., 2013] and has been used to examine research questions on climate engineering [e.g., *Lobell et al*., 2006; *Wilhelm et al*., 2015; *Xia et al*., 2016], climate extremes [e.g., *Fischer et al*., 2013; *Perkins and Fischer*, 2013], and irrigation [e.g., *Sacks et al*., 2009; *Thiery et al*., 2017].

The Community Earth System Model can be configured with different versions of the component models. We use the component set B20TRC5CN for the historical period 1850 to 2005 and BRCP85C5CN for the projections starting in 2006. More specifically, we use the Community Atmosphere Model version 5 [*Neale et al*., 2012] with 48 vertical levels, a time step of 1800s, and a horizontal resolution of 1.9° × 2.5°. The Community Atmosphere Model uses a finite volume dynamical core with terrain following hybrid sigma-pressure coordinates. Both ozone and volcanic aerosols are prescribed. Transient GHG emissions are used for all simulations, using historical emissions up to 2005 (atmospheric CO_2: 285 ppm to 379 ppm) and follow the Representative Concentration Pathway (RCP) 8.5 from 2006 onward (atmospheric CO_2: 380 ppm to 936 ppm). The Parallel Ocean Program version 2 is used to simulate ocean dynamics with 60 vertical levels and an hourly time step on a 1° × 1° Greenland-displaced polar grid. By using a fully coupled ESM, we are able to evaluate the effect of CeLM to counteract global warming.

The Community Land Model version 4 [*Oleson et al*., 2010; *Lawrence et al*., 2011] is used with the prognostic carbon-nitrogen biogeochemical model [*Thornton et al*., 2007] to represent the terrestrial processes that affect and are affected by climate through the exchange of energy and moisture between the land and atmospheric components of the Community Earth System Model. With the carbon-nitrogen submodel, the leaf and stem area indices and vegetation heights are calculated prognostically, and therefore, vegetation phenology is dynamic. Plant functional type (PFT) specific leaf growth and litterfall are a function of the day length and on the growing degree days exceeding critical temperature and moisture thresholds. There are 15 soil layers with increasing layer thicknesses from 0.018 m at the surface to 13.9 m for the deepest layer. Only the upper 10 layers are hydrologically active using a modified Richard's equation, while the bottom five layers are thermal slabs. To resolve the land surface heterogeneity, a subgrid tiling approach is used, where each grid cell is split into different land units to represent vegetated, urban, lake, wetland, and glacial surfaces. For vegetated surfaces, a single soil column is used, where up to 15 PFTs can coexist, each with their own set of parameters describing the optical, morphological, and photosynthetic properties of the vegetation class. The same atmospheric conditions are used to drive the land surface model for each land unit and PFT within the grid cell. The surface turbulent energy fluxes, radiative temperature, and albedo variables are calculated for each PFT and land unit independently before being aggregated to the grid cell level using the percent coverage of the grid cell to calculate a weighted average. In all simulations we use historical and projected transient land cover with land use change descriptions from *Hurtt et al*. [2006]. We do not use the prognostic crop model to limit computational costs. Furthermore, we do not use the dynamic vegetation mode as this only considers grass and tree PFTs [*Lawrence et al*., 2011].

The surface albedo is calculated for each PFT at the subgrid level for canopy and soil surfaces separately, which are then aggregated to a total surface albedo estimate as a weighted combination of snow-free and snow-covered albedos, where the weighting is determined by the snow cover fraction. All albedo terms are modeled using a two-stream approximation for radiative transfer to determine the direct and diffuse radiation contributions. There is also an irrigation parameterization enabled for a generic C3 crop PFT on its own soil column where all parameters are identical to the generic C3 crop PFT [*Oleson et al*., 2013]. Irrigation is only triggered during the growing season and when water is limiting for evapotranspiration. The irrigation rate is calculated as the total water deficit across the topmost unfrozen soil layers. This is

Table 1. Experimental Summary[a]

Configuration	Surface Albedo	Irrigation	Time Period
CTL		Off	1850–2099
ALB02	+0.02	Off	2020–2099
ALB04	+0.04	Off	2020–2099
ALB08	+0.08	Off	2020–2099
ALB10	+0.10	Off	2020–2099
IRRIG		On	2020–2099
IRRALB	+0.10	On	2020–2099

[a]All experiments consist of a three-member ensemble using transient land cover.

derived as the difference in current soil moisture content and a target with the latter calculated as a weighted combination of the soil moisture content eliminating water stress and the saturation soil moisture content. The irrigation rate is scaled according to the number of time steps to distribute the irrigated water over. In our study we use the default of nine time steps starting at 6 A.M. local time. Once the irrigation rate is calculated, it is added directly to the ground precipitation to mimic drip irrigation and subtracted from the total liquid runoff to mimic river water extraction. River extraction and irrigation are performed within the same time step to maintain the water balance. In this way, irrigation involves a redistribution of existing water stores at the land unit level.

2.2. Experimental Design

There are different CeLM schemes that could be pursued to achieve cooling; here we focus on crop albedo enhancement and irrigation. We run fully coupled simulations from 1850 to 2099, following RCP8.5 from 2006 onward. We choose RCP8.5 as this scenario has the largest GHG forcing and least amount of mitigation activity [*Riahi et al*., 2011]. Therefore, it is possible to evaluate the mitigation potential of CeLM under extreme conditions. Each configuration consists of a three-member ensemble that has been generated according to the approach detailed in *Fischer et al*. [2013], where a random perturbation of 10^{-13} is imposed in the atmospheric temperature initial conditions of the reference simulation. We run seven configurations (Table 1) consisting of a control (CTL) with no CeLM, four experiments (EXP) with different levels of crop albedo enhancement: +0.02, +0.04, +0.08, and +0.10 (denoted as ALB02, ALB04, ALB08, and ALB10, respectively), one experiment with irrigation enabled (IRRIG) and finally one experiment with both crop albedo enhancement of +0.10 and irrigation enabled (IRRALB) to evaluate if together they are complementary. In all experiments, CeLM is applied from 2020 and assumes no prior implementation; in this way it is possible to measure the effect of each CeLM scheme on climate independently. Although in reality irrigation is currently in use, our control simulation has no irrigation so that we can evaluate the cooling effect of irrigation independently from crop albedo enhancement.

The implementation of crop albedo enhancement follows the approach adopted by *Wilhelm et al*. [2015] where the subgrid level snow-free canopy albedo is increased for the generic C3 crop PFT by the different magnitudes noted above. As the vegetation phenology is dynamic, we further limit the crop albedo enhancement to periods when the leaf area index is nonzero. Therefore, crop albedo enhancement is not applied over periods when the leaf area index is zero or when there is snow. Furthermore, the albedo enhancement is only applied to the canopy albedo, not the background soil albedo. Therefore, conceptually we aim to represent the replacement of existing crops with those that are more reflective and do not consider how changes in canopy extent contribute to albedo changes by increasing exposure of bright soils and decreasing exposure of dark soils. This idealized approach is suitable to determine the upper limit that crop albedo enhancement can influence climate.

Albedo can vary between different cultivars of the same crop due to variations in leaf area index, leaf angle, background reflectance determined by soil color and moisture content, solar zenith angle, leaf reflectance, and canopy morphology [*Ridgwell et al*., 2009; *Singarayer et al*., 2009; *Doughty et al*., 2011]. In particular, within an existing crop type, leaf pubescence (i.e., hairs) and glaucousness (i.e., wax covering of leaves) properties can vary [*Doughty et al*., 2011]. *Grant et al*. [2003] report leaf level changes of reflectance of 0.05 in different sorghum cultivars as a result of different wax structures, while albedo variations of 0.01 due to changes in glaucousness have been measured in barley cultivars [*Febrero et al*., 1998]. *Uddin and Marshall* [1988] measure albedo variations across 28 wheat cultivars and report a range of 0.06 to 0.10 associated with changes in wax content. *Piggin and Schwerdtfeger* [1973] report seasonal changes in albedo of 0.12 for a single wheat cultivar

and 0.22 for a single barley cultivar that were attributed to changes in leaf area index and soil moisture. These higher estimates in albedo variation are likely to include the effects of changes in background soil reflectance. Further, canopy morphology has been shown to vary albedo by 0.08 for maize cultivars [*Hatfield and Carlson*, 1979]. *Breuer et al*. [2003] provide a comprehensive review of the literature of plant parameters including albedo. Typical albedo values for barley are 0.20–0.26, 0.16–0.26 for corn, 0.16–0.25 for oats, 0.11–0.25 for rye, 0.20–0.22 for soybean, 0.21–0.29 for sunflower, and 0.15–0.26 for wheat [*Breuer et al*., 2003]. Therefore, albedo variations within the same crop type can range from 0.01 to more than 0.10. However, lower values are more plausible as these observed plant scale albedo changes between cultivars may translate into different estimates at an ecosystem level due to differences in solar angle, background soil albedo, and direct and diffuse scattering of radiation. Therefore, we evaluate crop albedo enhancement values of +0.02, +0.04, +0.08, and +0.10 to reflect the plausible changes of albedo by changing cultivars within the same crop type. Changes in albedo across crop types can be larger; however, we advocate changing varieties within the same crop type to avoid significant disruption to food production. Observed changes in soil albedo of 0.10 associated with no till for a winter wheat crop [*Davin et al*., 2014] suggest another way to augment cropland albedo in addition to changing crop varieties. Therefore, we also consider albedo enhancement of +0.10 as the maximum possible albedo change for existing crops. Although changes in albedo are possible by changing the crop cultivars, there is limited knowledge on what this means for crop yield. However, new crop cultivars that are brighter and have better water use efficiency without compromising on crop yield are currently in development [e.g., *Drewry et al*., 2014; *Zamft and Conrado*, 2015]. In contrast, for no-till farming a metaanalysis from *Pittelkow et al*. [2015] suggests that although no till is more effective over dry climates with potential crop yield increases, decreases in crop yield are possible over more humid climates.

In the Community Land Model version 4.0, irrigation is only possible for fixed land cover of the year 2000. This is due to challenges in conserving water in the soil column with changing land cover and also associated with existing observations of the spatial extent to which irrigation is currently in use. As we use transient simulations, we had to make modifications to the PFT distributions to enable irrigation in transient land cover simulations. Here we use the transient distributions of the standard generic C3 crop PFT rather than the irrigated crop PFT commonly used in the fixed land cover configuration. The generic C3 crop PFT shares the same soil column as other PFTs, and therefore, all PFTs on this soil column can potentially benefit from the water added through irrigation when it is triggered. To limit the effect of irrigation on the noncrop PFTs we use a threshold of 50% cover of the C3 crop PFT. In this way irrigation is applied to the entire crop fraction but only when crops are the dominant vegetation cover and when the conditions for triggering irrigation (i.e., growing season and water stress) are met. Consequently, all simulated experiments are highly idealized and present a hypothetical scenario for the future implementation of CeLM over global agricultural regions. Therefore, we compare the relative impact of each approach: crop albedo enhancement or irrigation, on surface climate over the period 2020 to 2099 and leave issues relating to the plausible large-scale implementation of CeLM to the discussion section.

2.3. Analysis

Our analysis uses the ensemble average daily output from our climate model to examine changes in the extremes indices as defined by the Expert Team on Climate Change Detection and Indices [*Zhang et al*., 2011]. These indices include the annual maximum daytime temperature (TXx), the annual minimum nighttime temperature (TNn), the largest number of consecutive dry days (CDD) with precipitation below 1 mm, the maximum 1 day precipitation rate (R×1day) and the maximum 5 day precipitation (R×5day). We also examine changes in the monthly mean daytime maximum (T_{MAX}) and nighttime minimum temperatures (T_{MIN}) over the period 2020 to 2099 to evaluate changes in the temperature distribution. Unless noted, all analyses use the ensemble mean.

To examine changes in surface temperature (T_{sfc}) in response to CeLM we use a surface energy balance decomposition method adapted from *Luyssaert et al*. [2014]. Here we express the surface energy balance as

$$\varepsilon\sigma T_{sfc}^4 = SW_N + LW_D + Q_E + Q_H + \text{Residual} \quad (1)$$

Where ε is the surface emissivity, σ is the Stefan-Boltzmann constant ($5.67 \times 10^{-8}\,W\,m^{-2}\,K^{-4}$), SW_N is the net shortwave radiation, LW_D is the downward longwave radiation, Q_E is the latent heat flux and Q_H is the sensible

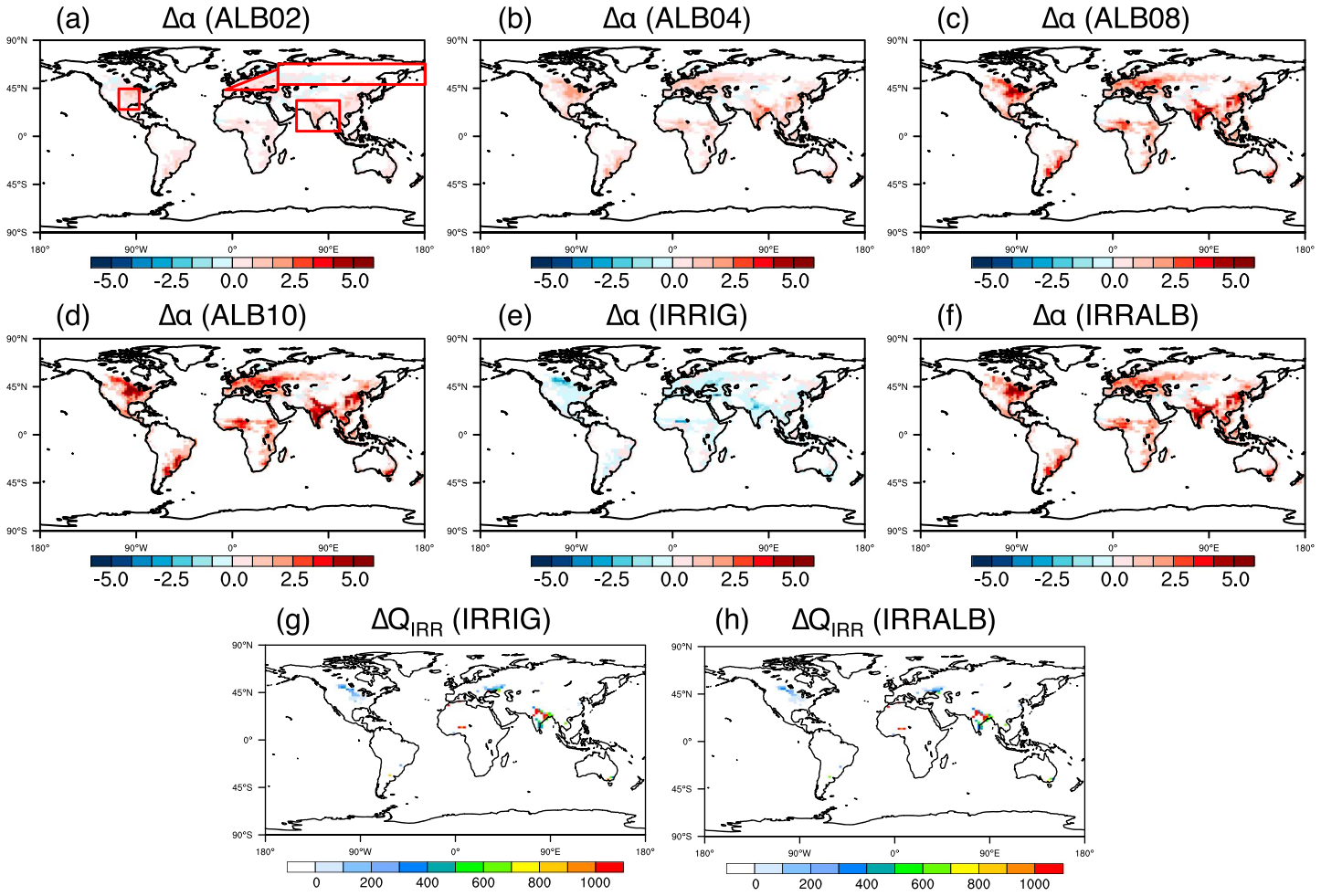

Figure 1. Contour map showing the mean applied forcing (EXP minus CTL) over 2020–2099: (a–f) the grid-scale surface albedo ($\alpha = 100 \times SW_U/SW_D$; %) and (g–h) the irrigation amount (Q_{IRR}; mm yr^{-1}). For experiments: ALB02 (Figure 1a), ALB04 (Figure 1b), ALB08 (Figure 1c), ALB10 (Figure 1d), IRRIG (Figures 1e and 1g), and IRRALB (Figures 1f and 1h). All maps are derived using the three-member ensemble mean of each configuration. Note that changes over the oceans have been masked. The red boxes in Figure 1a denote the four SREX regions presented in subsequent figures: Central North America (CNA), Central Europe (CEU), North Asia (NAS), and South Asia (SAS).

heat flux. The residual term includes the ground heat flux and changes in subsurface heat storage. The change in T_{sfc} can be calculated by taking the derivative of equation (1) with respect to T_{sfc} and solving for ΔT_{sfc}:

$$\Delta T_{sfc} = \frac{1}{4\varepsilon\sigma T_{sfc,CTL}^3}(\Delta SW_N + \Delta LW_D - \Delta Q_E - \Delta Q_H - \Delta \text{Residual}), \quad (2)$$

where Δ denotes the change between the experiment and the control (EXP minus CTL).

To examine regional changes we focus our analysis on the regions defined in the IPCC Special Report on Managing the Risks of Extreme Events (SREX) [*IPCC*, 2012; *Seneviratne et al.*, 2012]. Of these SREX regions, we present the results for Central Europe (CEU), Central North America (CNA), North Asia (NAS), and South Asia (SAS) (Figure 1a). CEU, CNA, and SAS were selected on the basis that they have intense agricultural activity and also coincide with regions where land-atmosphere coupling is strong [e.g., *Seneviratne et al.*, 2010]. NAS is included to provide an example of regions where the agricultural intensity, and thus the potential for CeLM, is comparatively low.

3. Results

3.1. Global Scale Response

We first present the applied forcing of each of the experiments in terms of the mean change (EXP minus CTL) in the grid-scale surface albedo ($\alpha = SW_U/SW_D$; Figures 1a–1f) and the irrigation amount (Figures 1g–1h) over

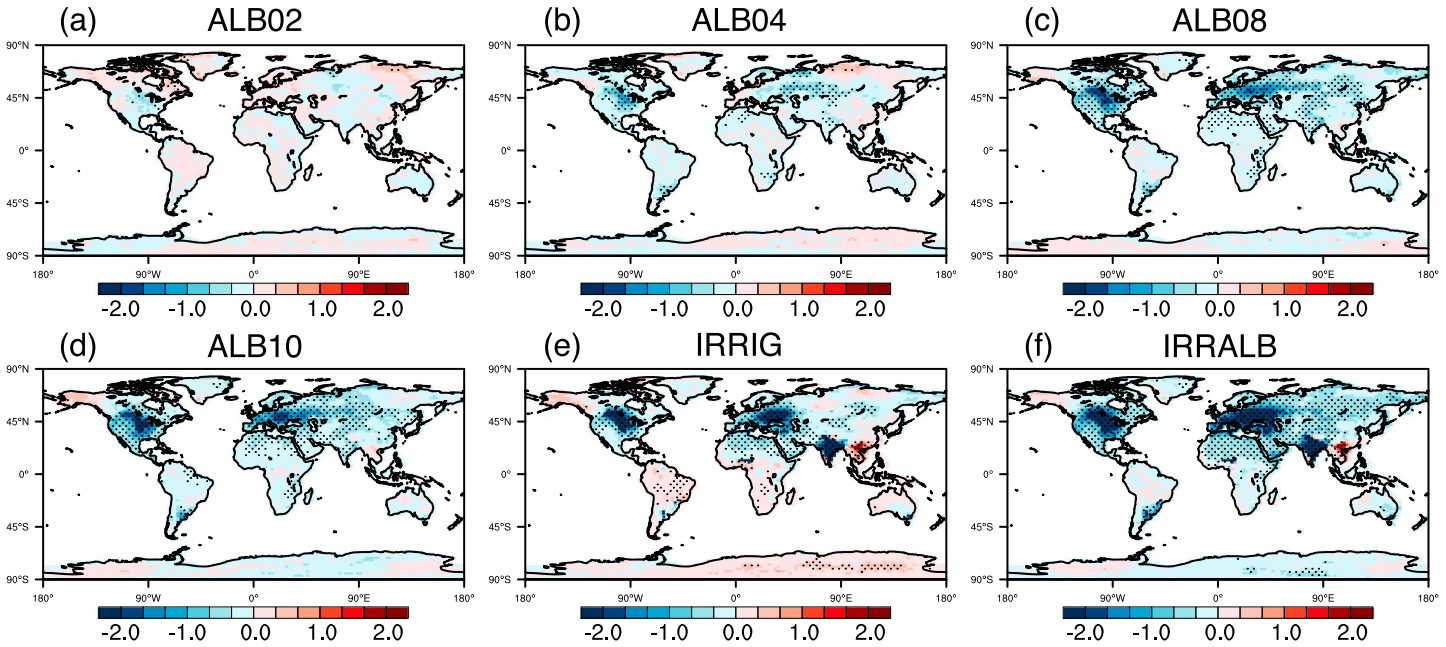

Figure 2. Contour map showing the mean change (EXP minus CTL) in the annual maximum daytime temperature (TXx; °C) over 2020–2099. For experiments: (a) ALB02, (b) ALB04, (c) ALB08, (d) ALB10, (e) IRRIG, and (f) IRRALB. All maps are derived using the three-member ensemble mean of each configuration. Note that changes over the oceans have been masked. Stippling indicates regions where the change is statistically significant at the 95% confidence level (determined from a 1000 bootstrap sampling procedure with a two-sided test of the paired difference between two means).

2020–2099. The grid-scale surface albedo increases with the scale of crop albedo enhancement over the major agricultural regions in all experiments where it is applied (i.e., ALB02, ALB04, ALB08, ALB10, and IRRALB). Indeed, there is a slight decrease (~2–4%) in the grid-scale surface albedo in IRRIG (Figure 1e) coincident with regions where irrigation is applied (e.g., Figures 1g–1h). This is likely due to how the soil albedo is calculated in the Community Land Model, where it is a function of the soil color and soil moisture content [*Oleson et al*., 2013]. The irrigation amounts applied over 2020–2099 show that irrigation is triggered over Central North America, Argentina, the Sahel, Eurasia, India, and Southeast Australia. The mean global irrigation amount is 2430 $km^3\,yr^{-1}$ (±143 $km^3\,yr^{-1}$) for IRRIG and 2222 $km^3\,yr^{-1}$ (±143 $km^3\,yr^{-1}$) for IRRALB. In the context of the observed quantity applied today of 2664 $km^3\,yr^{-1}$ [*Sacks et al*., 2009], the amounts of irrigation applied in our simulations are comparable to the present-day irrigation rates and fall within the range of observational uncertainty. However, the spatial extent is less than the present day spatial distribution [e.g., *Sacks et al*., 2009] due to the constraint we impose in our simulations to limit irrigation to where crops are the dominant vegetation cover. Therefore, it is possible that the mitigation potential of irrigation is underestimated by not including all regions where irrigation is currently practiced or the potential expansion of irrigation to regions where crops are currently rainfed.

Although the forcing is similar between the ensemble members of a given experiment, estimates of the change in the annual maximum daytime temperature (TXx) over 2020–2099 from individual simulations were noisy (not shown). These were substantially improved when examining changes in TXx from the ensemble mean, particularly over regions where the forcing is greatest (Figure 2). More specifically, the magnitude of the crop albedo enhancement (Figures 2a–2d) is critical for obtaining a robust cooling response. For example, ALB02 (Figure 2a) tends to experience more warming than cooling; however, most TXx changes are within ±0.3°C and generally not statistically significant. For ALB04 (Figure 2b), TXx decreases by ~1°C over North America and between 0.5°C and 1°C over Eurasia. These regions expand in ALB08 (Figure 2c) and ALB10 (Figure 2d) with a decrease in TXx of 1–2°C. While the application of crop albedo enhancement can be spatially constrained, the effects on climate are not entirely bounded to those regions, with some nonzero changes occurring over regions where limited or no albedo changes were applied. For IRRIG (Figure 2e) there is cooling of more than 2°C over North America, Eurasia, and India, but warming of ~1°C over Southeast Asia and Southern China. This warming of TXx is symptomatic of changes in monsoon precipitation (see

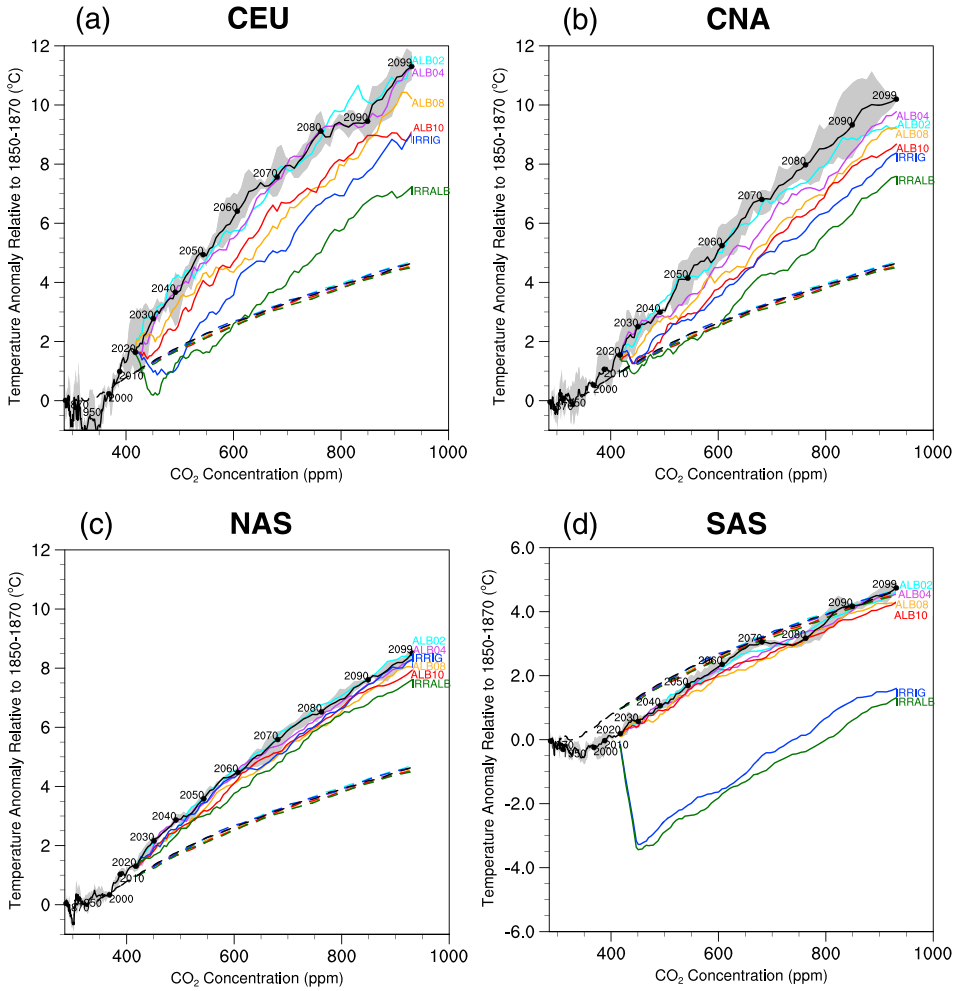

Figure 3. Regional temperature scaling with CO_2 concentration (ppm) over 1850 to 2099 for four different SREX regions: (a) CEU, (b) CNA, (c) NAS, and (d) SAS. Solid lines correspond to the regional average annual maximum daytime temperature (TXx) anomaly, and dashed lines correspond to the global mean temperature anomaly, where all temperature anomalies are relative to 1850–1870 and units are in °C. The black line in all panels denotes the three-member control ensemble mean with the grey-shaded regions corresponding to the ensemble range. The colored lines correspond to the three-member ensemble means of ALB02 (cyan), ALB04 (purple), ALB08 (orange), ALB10 (red), IRRIG (blue), and IRRALB (green).

Figures S1 to S4 in the supporting information). The cooling over North America, Eurasia, and India increases and expands further in IRRALB (Figure 2f), where TXx decreases by more than 2°C. Therefore, IRRALB appears to have the most robust cooling response of all the experiments.

3.2. Regional Scale Response

Between all the experiments, the regional differences are subtle and best illustrated by examining the regional trend in the TXx anomaly relative to 1850–1870 as a function of the CO_2 concentration (Figure 3). We focus on four different IPCC SREX regions: Central Europe (CEU), Central North America (CNA), North Asia (NAS), and South Asia (SAS) and examine changes across the land surface encompassed by each region. All panels in Figure 3 include the change in the global mean temperature anomaly (ΔT_{GM}; dashed lines) for each configuration. The change in ΔT_{GM} between all experiments is negligible (i.e., dashed lines overlap), demonstrating that the changes in temperature induced by the CeLM schemes examined here do not substantially change the global mean temperature but do affect temperature at regional scales. Figure 3 illustrates the importance of the magnitude of the crop albedo enhancement, complementing the results of Figures 2a–2d. In particular, for CEU (Figure 3a) ALB02 and ALB04 are barely distinguishable from the CTL ensemble range, while ALB08 and ALB10 have comparable decreases in the TXx anomaly. Similarly for CNA

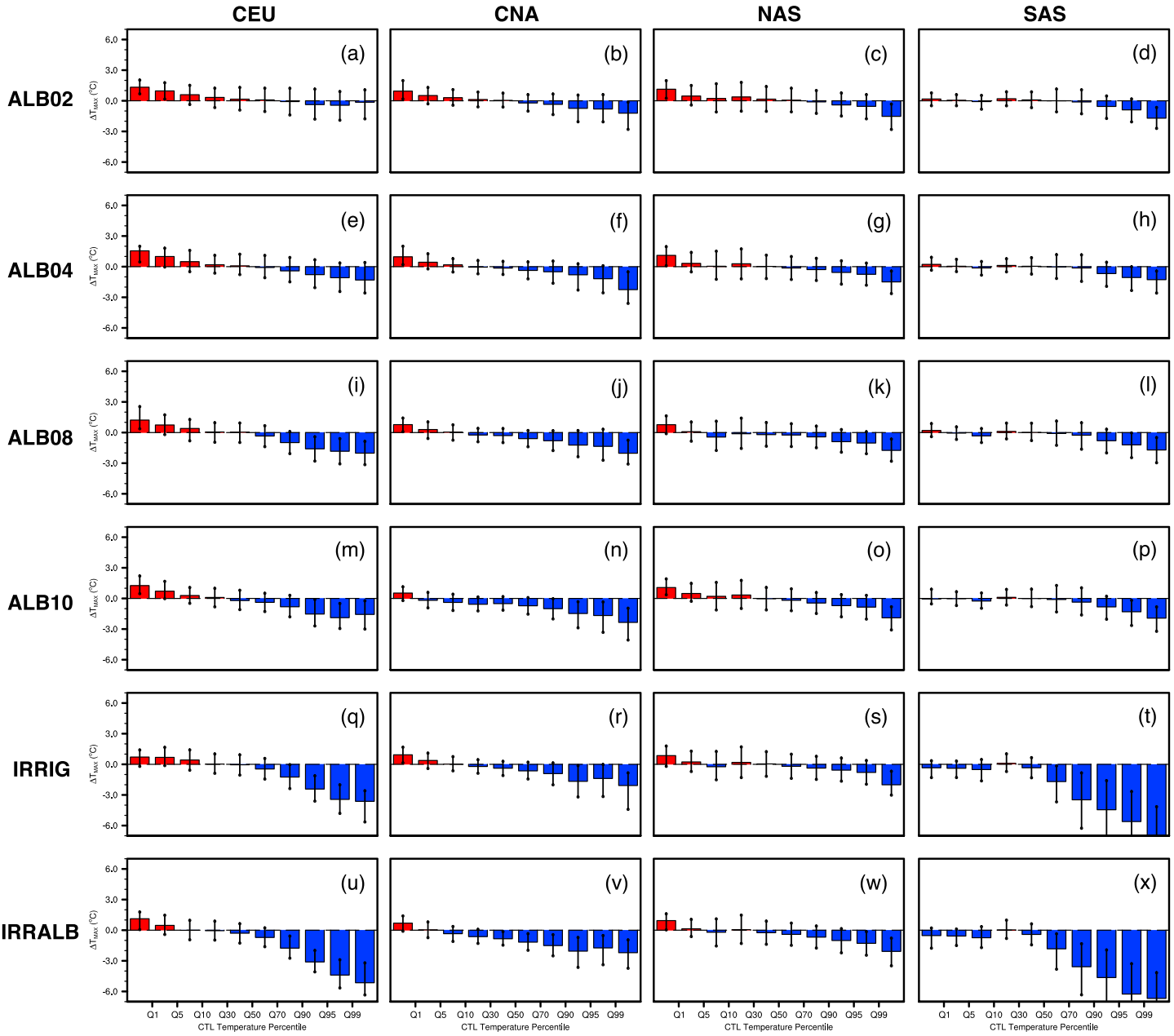

Figure 4. Median change (EXP minus CTL) in monthly mean daytime temperature (T_{MAX}; °C) over the boreal summer (June–August) months of 2020–2099 for four different SREX regions: (a, e, i, m, q, and u) CEU, (b, f, j, n, r, and v) CNA, (c, g, k, o, s, and w) NAS, and (d, h, l, p, t, and x) SAS. For experiments: ALB02 (Figures 4a–4d), ALB04 (Figures 4e–4h), ALB08 (Figures 4i–4l), ALB10 (Figures 4m–4p), IRRIG (Figures 4q–4t), and IRRALB (Figures 4u–4x). All data are binned according to the T_{MAX} percentiles of the (three-member) control ensemble mean. Blue indicates a cooling response, red indicates warming, and the bars denote the spatial interquartile range.

(Figure 3b), larger increases in albedo are necessary to distinguish the cooling potential of crop albedo enhancement from the CTL ensemble range. For NAS and SAS (Figures 3c and 3d), all levels of crop albedo enhancement are barely distinguishable from the CTL ensemble range, although there is a subtle decrease in the TXx anomaly with increased crop albedo enhancement.

Comparing between the different CeLM schemes: crop albedo enhancement (ALB10), irrigation (IRRIG), and both (IRRALB) illustrate that there are differences in the cooling potential of TXx. For CEU (Figure 3a), ALB10 contributes a ~1°C decrease in the TXx anomaly over 2020–2099, IRRIG contributes a ~2°C decrease, and

IRRALB contributes a ~3°C decrease in the TXx anomaly. Indeed, for IRRALB the trajectory of the TXx anomaly is below ΔT_{GM} up until 2060. For CNA (Figure 3b) both ALB10 and IRRIG show comparable decreases in the TXx anomaly of ~1.5°C until 2070. The TXx anomaly for IRRALB also follows ΔT_{GM} until 2060. For NAS (Figure 3c), the change in the TXx anomaly is limited, although decreases achieved in ALB10 are marginally greater than IRRIG, and changes by ~ −0.5°C for IRRALB. In contrast, for SAS (Figure 3d) the change in TXx from irrigation is considerable, with a decrease of the TXx anomaly of ~3°C for IRRIG and IRRALB. Figure 3 demonstrates that the efficacy of CeLM is region dependent and that no scheme can maintain regional temperature extremes within the global mean temperature anomaly over the entire period 2020–2099. Therefore, CeLM cannot offset global warming. Finally, the application of both crop albedo enhancement and irrigation (IRRALB) generally achieves the largest decrease in the TXx anomaly across all regions shown here, despite their respective different mechanisms for achieving cooling (see section 3.4).

3.3. Changes in Temperature Distribution

Given the changes in TXx shown in Figures 2 and 3, it is anticipated that the impact of CeLM is not constrained to changing the upper tail of the temperature distribution. Using monthly mean daytime temperatures (T_{MAX}) we examine the change (EXP minus CTL) in the daytime temperature distribution over the summer months when CeLM is active in all experiments (Figure 4). Here all data are binned according to different percentiles with the bin edges at the 1st, 5th, 10th, 30th, 50th (median), 70th, 90th, 95th, and 99th percentiles of the CTL ensemble mean. All data points (through space and time) within a region are ranked to determine the median and interquartile range of the change for each bin. Again, we focus on the same SREX regions as in Figure 3: CEU, CNA, NAS, and SAS (corresponding to the columns) and the different experiments (corresponding to the rows). Generally, the cooling response in most experiments (particularly in Figures 4i–4x) is greatest for the hot temperature extremes (i.e., Q90, Q95, and Q99) than the median (i.e., Q50). For example, cooling over CEU for ALB10 (Figure 4m) increases in magnitude from −0.5°C at the median (Q50) to −2°C for the highest percentile (Q99); however, there is also a warming response for the lowest percentile of +1.5°C (Q1). In fact this is generally true in most panels of Figure 4, except for those corresponding to SAS. In particular, for small levels of crop albedo enhancement (e.g., ALB02 and ALB04; Figures 4a–4c and 4e–4g), the warming of the lower percentiles (Q1, Q5, and Q10) often offsets any cooling achieved in the upper percentiles (Q90, Q95, and Q99). This is consistent with the results of Figures 3 where ALB02 and ALB04 were rarely distinguishable from the CTL ensemble range. This suggests that small levels of crop albedo enhancement are unlikely to achieve a robust cooling effect.

Besides changing the planetary albedo, the application of CeLM also forces a redistribution of energy within the climate system. Therefore, it is not unexpected that cooling of hot temperature extremes (Q90, Q95, and Q99) results in warming of cool temperature extremes (Q1, Q5, and Q10). However, we also find that warming of the lower percentiles can be greater over the winter months when CeLM is not active (see example in Figure S5 of the supporting information). Therefore, the affect of CeLM on extremes is not entirely symmetrical due to how feedbacks within the climate system exacerbate temperature extremes through changes at the surface and in the boundary layer. To understand why CeLM has the potential to induce warming, we examine the change in the radiative fluxes, cloud cover, and the turbulent heat fluxes. We show the results for CEU over the summer months for the ALB10 (Figure 5) and IRRIG (Figure 6) experiments; however, both CNA and NAS showed similar responses (not shown) and SAS showed negligible warming of the lower temperature percentiles.

Over boreal summer (June–August; JJA) changes in the grid-scale surface albedo is consistent with the imposed forcing (e.g., Figure 1) with an increase in albedo (3%) for all maximum temperature percentiles for ALB10 (Figure 5a) and a subtle decrease (−1%) for IRRIG for the highest temperature percentile (Q99; Figure 6a). Increasing the surface albedo decreases the net available energy at the surface, and irrigation changes the potential evaporation. Therefore, the latent (Q_E) and sensible (Q_H) heat fluxes are likely to change, particularly over the months when crop albedo enhancement or irrigation is applied. More specifically, Q_E generally increases over JJA for the highest percentiles (Q90, Q95, and Q99) particularly for IRRIG (10–30 W m^{-2}; Figure 6b) and also by a smaller amount for ALB10 (5–10 W m^{-2}, Figure 5b) indicative of more evaporative cooling at the surface. This is enhanced by a corresponding decrease in Q_H in both experiments, particularly for the highest percentiles (5–20 W m^{-2}, Figures 5c and 6c), reflecting either the decrease in net available energy (e.g., ALB10) or the increase in latent heating (e.g., IRRIG and also ALB10). These changes in

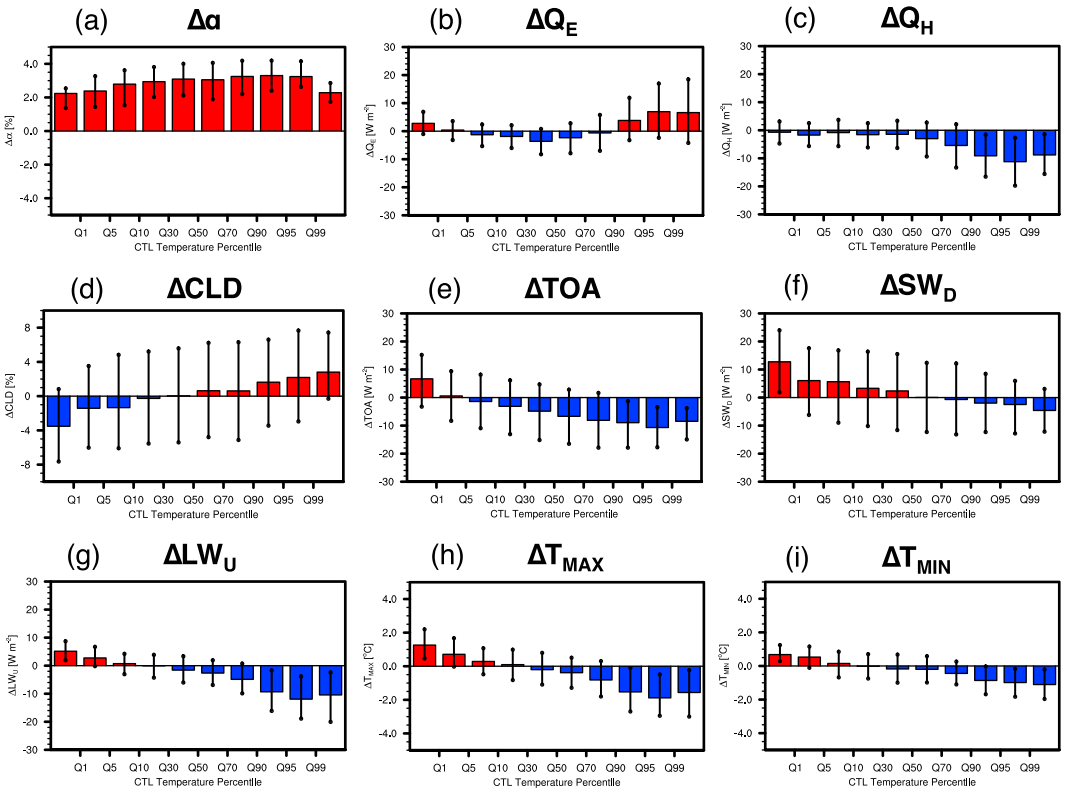

Figure 5. Examination of the warming response of cool temperatures in the ALB10 experiment. Example for CEU over boreal summer (June–August). Median change (EXP minus CTL) over 2020–2099 in the (a) grid-scale surface albedo ($\alpha = 100 \times SW_U/SW_D$; %), (b) latent heat flux (Q_E; W m^{-2}), (c) sensible heat flux (Q_H; W m^{-2}), (d) total cloud fraction (CLD; [0 1]), (e) net flux at top of the atmosphere (TOA; W m^{-2}), (f) downward shortwave radiation (SW_D; W m^{-2}), (g) emitted longwave radiation (LW_U; W m^{-2}), (h) maximum (daytime) temperature (T_{MAX}; °C), and (i) minimum (nighttime) temperature (T_{MIN}; °C). All data are binned according to the T_{MAX} percentiles of the (three-member) control ensemble mean. The bars denote the spatial interquartile range.

Q_E and Q_H have implications for boundary layer development and cloud cover. The increase in Q_E contributes to more water vapor available for cloud formation with increasing cloud cover in both experiments for the highest percentiles (4–6%, Figures 5d and 6d). However, for the lowest percentile (Q1) cloud cover decreases by ~4% in ALB10 and ~2% in IRRIG. The change in the net flux at the top of the atmosphere in both experiments (Figures 5e and 6e) also reflects these changes in cloud cover, with decreases of 5–10 W m^{-2} coincident with the increase in cloud cover for the highest percentiles. These changes in cloud cover have a corresponding effect on the downward shortwave radiation (SW_D) of both ALB10 and IRRIG. More specifically, for the highest percentiles (Q95 and Q99) SW_D decreases by 5–10 W m^{-2} in both experiments (Figures 5f and 6f), indicative that increased cloud cover reflects more downward shortwave radiation above the cloud layer. Conversely, the decrease of 2–4% of cloud cover for the lower percentiles (Q1 and Q5) in both experiments contributes to an increase of 5–10 W m^{-2} in SW_D. The changes in cloud cover do affect the energy available at the surface, where there is a decrease in longwave emission (LW_U) at the surface (Figures 5g and 6g). In particular, for the highest percentiles (Q95 and Q99), when there is more cloud cover LW_U decreases by 10–20 W m^{-2} and for the lowest percentiles (Q1 and Q5) LW_U increases by ~5 W m^{-2}. The daytime (T_{MAX}, Figures 5h and 6h) and nighttime (T_{MIN}, Figures 5i and 6i) temperature response to CeLM is consistent with the changes in the surface turbulent fluxes and radiative fluxes. For the highest percentiles (Q90, Q95, and Q99), T_{MAX} decreases by 1–3°C as a result of the increase in Q_E and decrease in Q_H but further enhanced by the increase in cloud cover that reflects more downward shortwave radiation and therefore reduces the amount of energy available at the surface. T_{MIN} also decreases by 1–2°C for the highest percentiles as a result of decreases in longwave emission. For the lowest percentiles (Q1 and Q5) the increase in T_{MAX} and T_{MIN} of ~0.5–1°C can be explained by the

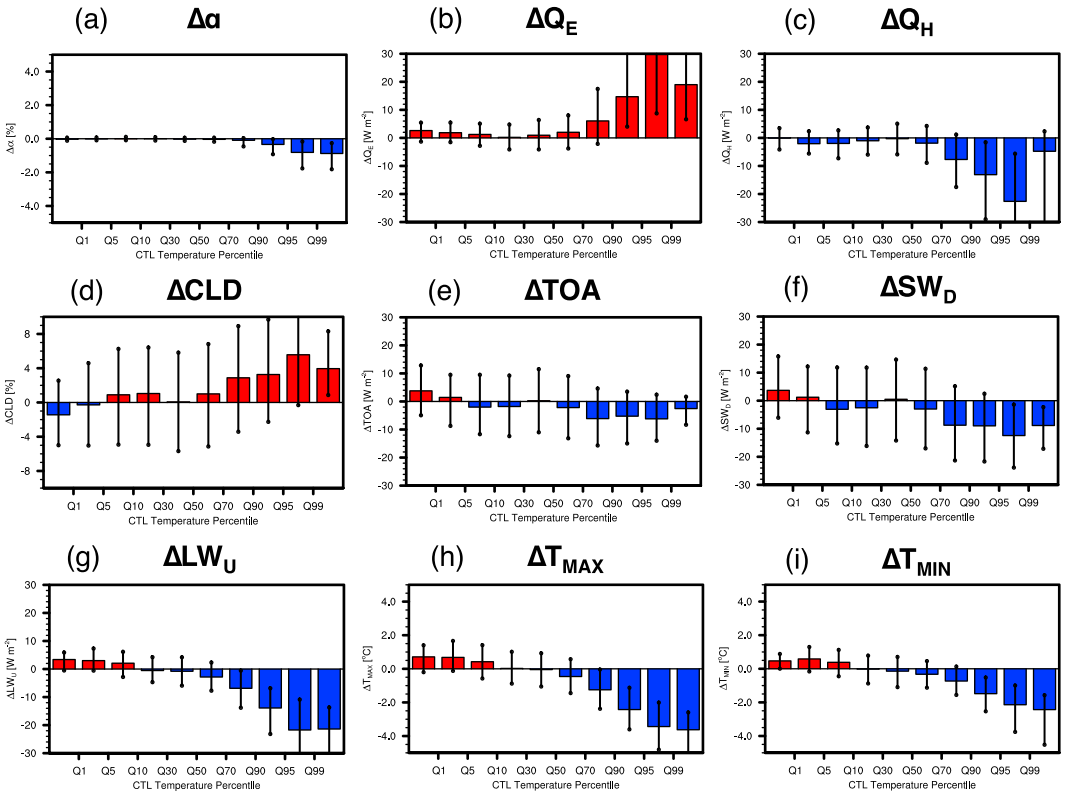

Figure 6. As is Figure 5 but for the IRRIG experiment.

decrease in cloud cover which enables more shortwave radiation to reach the surface. Therefore, changes in the temperature distribution reflect changes in available energy that are at first an immediate response to direct changes in the surface energy balance from CeLM that then evolve to influence cloud cover.

We note here that the increase in cloud cover over the summer months does not dissipate at the end of the growing season when CeLM ceases. Rather, the increased cloud cover persists over the winter months. Over the winter months the climate system does not fully return to an unperturbed state due the changes in the hydrological cycle that are initiated over the period when CeLM is active. The hydrological response takes longer relative to the instantaneous changes in available energy through albedo change upon the cessation of CeLM. Increased cloud cover during winter thus leads to additional warming through increased LW_D (Figure S5).

We also checked the change in minimum temperature (T_{MIN}) and the annual minimum nighttime temperature (TNn; Figures S6 and S7 in the supporting information). Generally, T_{MIN} decreases between −0.2°C and −1°C over the same regions of North America, Eurasia, and India where TXx (and T_{MAX}; Figure S8) decreases. However, T_{MIN} increases of more than +0.5°C are found in ALB02 and also in IRRIG over regions where irrigation was not enabled. Similar spatial patterns are found with TNn, although the decreases and increases are generally larger in magnitude than those for T_{MIN}. The decrease in T_{MAX} is generally larger than the decrease in T_{MIN} and therefore there is a narrowing of the diurnal temperature range of ~1°C over North America, Europe, and India for the ALB10, IRRIG, and IRRALB experiments (Figure S9). Over Southeast Asia in IRRIG and IRRALB the diurnal range increases by more than 1°C where changes in monsoon precipitation were evident (Figure S2 to S4).

3.4. Mechanisms for Regional Differences

Figure 3 demonstrated that the CeLM schemes lead to different magnitudes of TXx cooling where either irrigation (e.g., CEU, Figure 3a) or crop albedo enhancement (e.g., NAS, Figure 3c) was more effective at reducing TXx, or both were comparable for part of the period 2020–2099 (e.g., CNA, Figure 3b). A similar pattern

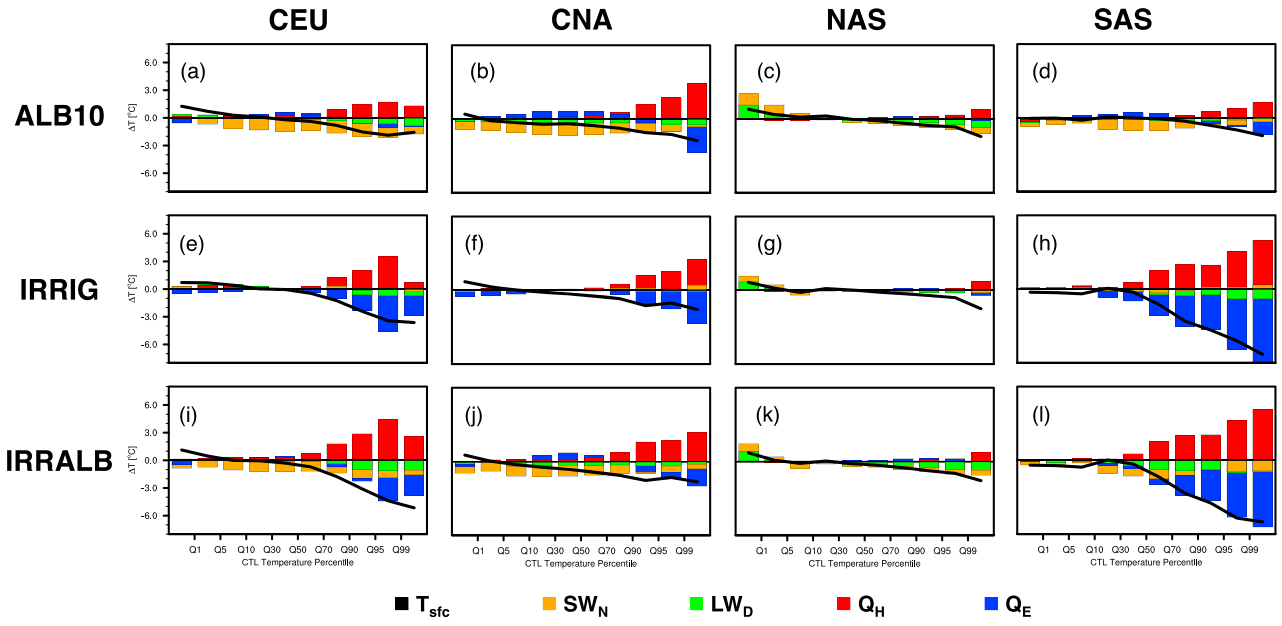

Figure 7. Change (EXP minus CTL) surface temperature explained by changes in the net shortwave radiation (SW_N; orange), downward longwave radiation (LW_D; green), sensible heat flux (Q_H; red), and the latent heat flux (Q_E; blue) over 2020–2099 for four different SREX regions: (a, e, and i) CEU, (b, f, and j) CNA, (c, g, and k) NAS, and (d, h, and l) SAS. For experiments: ALB10 (Figures 7a–7d), IRRIG (Figures 7e–7h), and IRRALB (Figures 7i–7l). All data are binned according to the T_{MAX} percentiles of the (three-member) control ensemble mean. The black line denotes the median change in surface temperature for each region.

emerges when comparing the changes in the T_{MAX} distribution between ALB10 and IRRIG (Figures 4m–4t). To understand why these regional differences exist, we consider how each CeLM scheme, crop albedo enhancement, and irrigation changes the surface energy balance. Crop albedo enhancement achieves cooling initially by decreasing the amount of energy available at the surface (e.g., Figure 5a), contributing to a decrease in Q_H (Figure 5c) and partly in Q_E (Figure 5b). However, changes in the partitioning between Q_H and Q_E also occur and lead to an increase Q_E, particularly for the higher percentiles (Q90, Q95, and Q99, Figure 5b). This in turn leads to enhanced water vapor in the lower atmosphere that triggers an increase in cloud cover (Figure 5d). The increase in cloud cover further limits downward shortwave radiation (Figure 5f), thus acting as a positive feedback for surface cooling. Irrigation achieves cooling by increasing the evaporative fraction (Figure 6b). This change in the partitioning between Q_H and Q_E also triggers an increase in cloud cover (Figure 6d) and associated decrease in downward shortwave radiation (Figure 6f), again leading to further cooling. Therefore, crop albedo enhancement triggers the change in the surface energy balance by altering the net energy available at the surface through albedo and irrigation changes the partitioning between Q_E and Q_H through increased soil moisture. To determine which flux triggers the largest change (EXP minus CTL) in surface temperature, we use the surface energy balance decomposition approach explained in section 2.3.

For CEU, irrigation was considered more effective at reducing TXx than crop albedo enhancement (e.g., Figure 3a). From the surface energy balance decomposition (Figure 7), temperature changes for CEU in ALB10 are mostly explained by changes in net shortwave radiation (ΔSW_N) and Q_H (Figure 7a) and by Q_E in IRRIG (Figure 7e). More specifically, for the highest percentile (Q99), in ALB10 (Figure 7a) ΔSW_N changes temperature by −2°C which is countered by a change of +1.5°C due to ΔQ_H. Downward longwave radiation (LW_D) also contributes to a −1°C change in temperature in ALB10. In contrast, temperature changes by −3°C in IRRIG for the highest percentile are mostly explained by ΔQ_E (Figure 7e). Similarly, in IRRALB (Figure 7i), temperature change is again mostly explained by changes in Q_E (−3.5°C) for the highest percentile (Q99). However, for lower temperature percentiles (Q5 to Q90), temperature changes are more often explained by changes in ΔSW_N (ALB10, Figure 7a and IRRALB, Figure 7i) indicative that irrigation is more effective for reducing TXx, but for the remainder of the temperature distribution, albedo change is also effective.

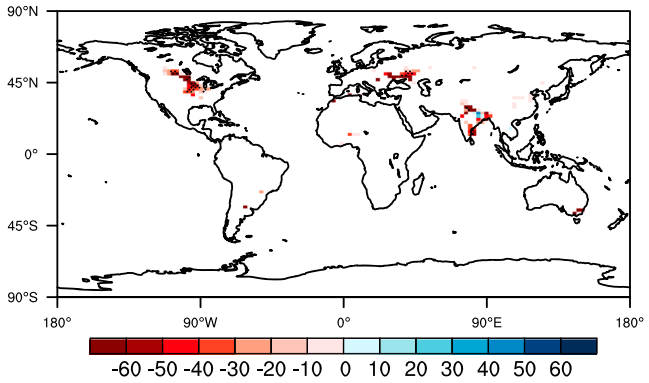

Figure 8. Contour map showing the mean change (IRRALB minus IRRIG) in irrigation amount (Q_{IRR}; mm yr^{-1}) over 2020–2099. Blue colors indicate more irrigation in IRRALB, and red colors indicate less irrigation in IRRALB. The contour map is derived using the three-member ensemble mean of each configuration. Stippling indicates regions where the change is statistically significant at the 95% confidence level.

For CNA both crop albedo enhancement and irrigation are comparable in their effect on reducing TXx over 2020–2070 (e.g., Figure 3b). For the highest percentile (Q99), temperature changes of −4°C in both ALB10 (Figure 7b) and IRRIG (Figure 7f) are due to ΔQ_E. However, ΔQ_H contributes a +4°C change in temperature in ALB10 and +3.5°C in IRRIG. For IRRALB (Figure 7j), temperature change of the highest percentile is also mostly attributed to ΔQ_H. Consequently, the actual change in temperature over CNA for the highest percentile is similar between ALB10, IRRIG, and IRRALB (−2.5°C) suggesting that of the CeLM schemes examined here, none has a substantial advantage above the others. As in CEU, CNA temperature changes of the lower percentiles (Q5 to Q90) tend to be explained by ΔSW_N (ALB10, Figure 7b and IRRALB, Figure 7j).

For NAS crop albedo, enhancement was often more effective at reducing TXx than irrigation (e.g., Figure 3c) in part because irrigation was rarely triggered over this region (e.g., Figure 1g). For ALB10 (Figure 7c) and IRRALB (Figure 7k) temperature change over NAS is mostly associated with ΔSW_N and ΔLW_D particularly for the tails of the temperature distribution (Q1, Q5, Q95, and Q99). For the highest percentile (Q99), ΔQ_H also contributes to +1°C in all experiments over NAS (Figures 7c, 7g, and 7k). Therefore, over NAS, changes in available energy are the critical driver of temperature change and these were largely determined by albedo change.

For SAS, irrigation has a substantial effect on TXx (e.g., Figure 3d) that is associated with the higher rates applied over the region (e.g., Figure 1g). In ALB10 (Figure 7d), IRRIG (Figure 7h) and IRRALB (Figure 7l), temperature change of the highest percentile (Q99) is dominated by changes in the partitioning between Q_E and Q_H. The actual temperature change in IRRIG and IRRALB is substantially larger than ALB10 (−6°C compared to −2°C) reflecting the larger changes in Q_E and Q_H.

Our results show that the largest cooling response over many regions is often possible when both crop albedo enhancement and irrigation are implemented (e.g., Figure 3). Given that crop albedo enhancement decreases the net available energy at the surface (e.g., Figures 5 and 7) and irrigation partitions more energy into evapotranspiration (Figures 6 and 7), the implementation of both over a long period is likely to have some impact on irrigation rates. Therefore, we examine the change in the irrigation amounts between IRRALB and IRRIG (Figure 8). Indeed, there are regions over North America, India, Eastern Eurasia, and Southeast Australia where there is a decrease (~25–60 mm yr^{-1}) in the mean annual irrigation amount over 2020–2099 when crop albedo enhancement is also applied. This suggests that irrigation frequency may be reduced if used in conjunction with crop albedo enhancement as the decrease in available energy reduces evaporative demand.

Given that there are regional differences in how much TXx can be reduced by CeLM, we examine which CeLM scheme, ALB10 or IRRIG, reduces TXx the most at the local grid-scale (Figure 9) rather than at the aggregated regional scale (e.g., Figures 3 to 7). To determine which is more effective at reducing TXx we define grid cells where there is "no preference" (yellow) when the average difference between the ALB10 and IRRIG TXx anomalies are within ±0.3°C. A "small impact" (white) is determined when the change in the TXx anomaly from both ALB10 and IRRIG is within ±0.3°C. The "albedo preference" (red) is defined when the average change in the TXx anomaly is larger in ALB10 than IRRIG. The "irrigation preference" (blue) is defined when the average change in the TXx anomaly is larger in IRRIG than ALB10. The choice of threshold is subjective, and indeed, using a threshold to 0.5°C increases the number of grid cells where there is excessive classification of either "no preference" or "small impact" from the CeLM schemes. Using a threshold to 0.1°C results in

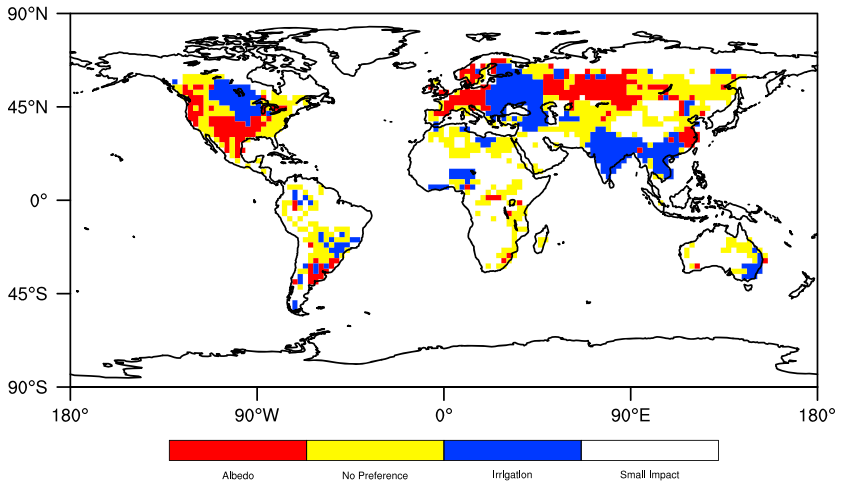

Figure 9. Contour map showing the climate-effective land management preference according to TXx reductions evaluated at each grid cell over 2020–2099. Preference is determined by calculating the mean change in the TXx anomaly between ALB10 and IRRIG. A threshold of 0.3°C is used to distinguish between small changes from crop albedo enhancement and irrigation or no preference. Legend: albedo preference (red), irrigation preference (blue), either albedo or irrigation (yellow), and small impact (white). Note that the oceans are also masked in white.

irrigation showing a larger reduction in TXx than crop albedo enhancement over regions where it is not applied. We also limit the analysis to crop regions where CeLM is applied to limit nonlocal effects. Regions where irrigation contributes to the largest decreases in TXx (Figure 9) tend to occur in the regions where irrigation is active (e.g., Eastern North America, Eastern Europe, India, Southeast Asia, and Southeast Asia). There is also some extension into other nonirrigated regions, suggesting that nonlocal cooling from irrigation is possible, which has been examined in *de Vrese et al*. [2016] and *Thiery et al*. [2017]. There are many regions where the effects of crop albedo enhancement and irrigation are comparable or have a small impact, particularly where the crop extent is limited and therefore the applied forcing is negligible (e.g., Amazon forest, Southern Africa, the Gobi Desert, and North East Australia). Regions where crop albedo enhancement is more effective at reducing TXx mostly coincide with regions where irrigation is not triggered in the model and include Western Europe, Scandinavia, Western Siberia, the Southern Great Plains, and Mexico. However, Figure 9 only illustrates where and which CeLM schemes reduce the TXx anomalies by the largest amount as determined by idealized experiments in the Community Earth System Model. Therefore, this is not prescriptive of where each CeLM scheme could be implemented, particularly if nonlocal effects are possible. Furthermore, other factors including water use efficiency may be equally important in addition to reductions in TXx which will be pursued in future research.

3.5. Implications for Vegetation Productivity

All CeLM schemes examined here involve some level of crop modification, and therefore, it is necessary to consider whether there are implications for crop yield. We interrogate the changes in net primary productivity (NPP, Figure 10, see Figure S10 for the percentage change) as a proxy for the vegetation response to CeLM. Note that here we use grid-scale estimates of NPP and not the PFT level values, as this would be prohibitively expensive to produce and examine. Consequently, we can only provide an overview of changes in vegetation productivity at the grid-scale level. In general, there is an increase in NPP over regions where there is a robust mean summertime cooling response (e.g., Figure 2). For ALB02 and ALB04 (Figures 10a and 10b), changes in NPP are generally within 5 gC m^{-2} yr^{-1} (~1 %) and not statistically significant; however, these experiments produced a weak cooling response. In contrast, over North America, Europe, and India, NPP increases by 15 gC m^{-2} yr^{-1} (~5 %) in ALB08 and ALB10 (Figures 10e and 10f) and by more than 30 gC m^{-2} yr^{-1} (>10 %) in IRRIG and IRRALB (Figures 10e and 10f). Over Southeast Asia and Southern China, NPP decreases by ~30 gC m^{-2} yr^{-1} (~5 %) in IRRIG and IRRALB (Figures 10e and 10f) coincident with where TXx increases (Figures 2e and 2f) and precipitation decreases (Figures S1 to S4). The changes in NPP overall suggest that the temperature reductions due to CeLM provide conditions that are more optimal for plant growth compared to a scenario without CeLM in our climate model.

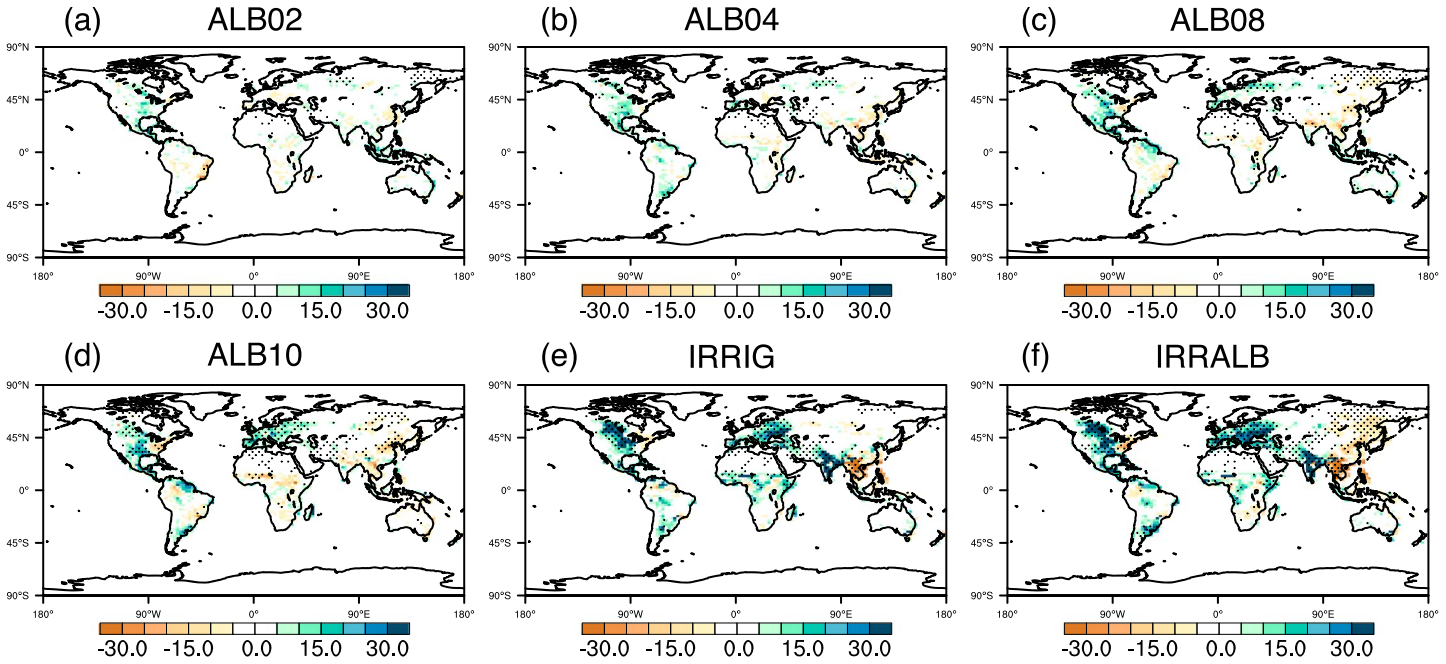

Figure 10. Contour map showing the mean change (EXP minus CTL) in the Net Primary Productivity (NPP; gC m^{-2} yr^{-1}) over 2020–2099. For experiments: (a) ALB02, (b) ALB04, (c) ALB08, (d) ALB10, (e) IRRIG, and (f) IRRALB. All maps are derived using the three-member ensemble mean of each configuration. Note that changes over the oceans have been masked. Stippling indicates regions where the change is statistically significant at the 95% confidence level.

4. Discussion

In this paper we examine the mitigation potential of CeLM to reduce regional warming of hot temperature extremes associated with anthropogenic climate change. We use the Community Earth System Model to run idealized global simulations for different levels of crop albedo enhancement, irrigation, and the application of both schemes to determine if there are regional preferences and why they exist. There are, however, three important caveats to our results. The first concerns the feasibility of large-scale implementation of CeLM, the second considers the mitigation potential, and the third discusses the model dependence of our results.

Feasibility is a prominent criticism of most climate engineering research using idealized climate model simulations. In the context of CeLM, this is also true. While it is possible to test an idea in a climate model, it may be difficult to implement in the real world. Our results show that a reduction of TXx greater than 0.5°C from crop albedo enhancement requires a large change in albedo of 0.08 or more (e.g., Figure 2) over extensive regions. Although significant variability of albedo exists among different varieties of the same crops [e.g., *Ridgwell et al.*, 2009], large-scale implementation may be the biggest challenge in terms of encouraging a diverse community of farmers to change to brighter crops particularly if there will be changes in yield or other unknown resource costs. Changes in other land management practices may also be required, such as no tillage, in order to supplement crop albedo enhancement to sufficient magnitudes, particularly after the growing season. However, our study does provide an upper limit on the potential CeLM has for reducing hot temperature extremes during the growing season. Given the changes in extremes due to CeLM future research efforts must aim to implement more rigorous parameterizations of land management in climate models, as well as the effect of CeLM at smaller spatial extents and the subgrid scale.

Our simulations also have no constraint on water availability for irrigation, meaning that when the conditions necessary to trigger irrigation are met, irrigation is always possible. We examined the water balance over each of the main irrigated regions of CEU, CNA, and SAS in our simulations (not shown). When irrigation is active in our model, the irrigation rate is of the same order at the total runoff (the irrigation source), indicating that these amounts can be applied, particularly if the presence of reservoirs is assumed. Therefore, the cooling from irrigation in our simulations is indicative of what is possible if there are no constraints on water

resources. However, in the real world water limitations associated with droughts, like the millennium drought experienced in Australia [*van Dijk et al*., 2013], impose limits on the ability to irrigate sustainably. Furthermore, *Feng et al*. [2016] find that the revegetation program of the Loess Plateau of China is actually contributing to an additional constraint on water availability due to increases in evapotranspiration reducing runoff into reservoirs. Therefore, water constraints on irrigation are likely to be exacerbated with climate change, where further changes in the hydrological cycle could affect the future distribution of water resources available for irrigation [*IPCC*, 2013]. Future research is planned to implement such constraints on irrigation to examine the long-term potential of irrigation in a 2°C (or more) world.

Our results focus on the mitigation potential of CeLM on hot temperature extremes and not cold temperature extremes or precipitation. However, the identification of a positive feedback on cloud development that contributes to temperature warming during the winter months when CeLM is temporarily suspended requires confirmation in other ESMs. In particular, the benefits of CeLM are perhaps negligible for regions where the summertime cooling from CeLM is offset by warming of comparable magnitudes in winter. Changes in temperature due to cloud cover over months when CeLM is not active may be resolved if no till is employed after the growing season to minimize the change in albedo between seasons; however, this hypothesis requires further investigation. Termination effects in other climate engineering schemes have been identified, with the most severe consequences associated with stratospheric aerosol injection [e.g., *Aswathy et al*., 2015; *Curry et al*., 2014; *Crook et al*., 2015]. However, to our knowledge our study is the first to consider the impacts of temporary cessation of CeLM. Before any real-world application of CeLM can be considered, more research is required to quantify the risk of negative impacts from temporary suspension or complete cessation of CeLM.

Further limitations on the mitigation potential of CeLM pertain to the experimental design where we compare all experiments to a control where there is no irrigation, despite the fact that irrigation already exists now. Therefore, the mitigation potential from irrigation is perhaps already realized in the past and can only be increased by expanding to regions where irrigation is currently not employed. However, this expansion will depend critically on the sustainable use of future water resources. Another unknown consequence of CeLM is whether there will be changes in crop yield. Although we find increases in NPP suggesting more productive vegetation, we cannot state if this means yields will also increase. The effect of stratospheric aerosol injection on vegetation has been examined in *Xia et al*. [2016] and *Glienke et al*. [2015] who find an increase in NPP due to increases in diffuse radiation and cooling associated with stratospheric aerosol injection. However, in the context of CeLM, not enough is known on whether brighter crops yield bigger harvests.

Finally, we cannot exclude the model dependence of our results. Previous studies examining the potential of crop albedo enhancement using the same model have found similar cooling responses to those reported here [e.g., *Lobell et al*., 2006; *Wilhelm et al*., 2015]. We find that the potential of land-based schemes relative to climate engineering schemes has been understated in previous research due to the focus on climate means rather than extremes. Furthermore, we are not the first to examine the impact of climate engineering on extremes or identify an asymmetric response of temperature extremes to climate engineering [e.g., *Curry et al*., 2014; *Davin et al*., 2014; *Aswathy et al*., 2015; *Wilhelm et al*., 2015]. In particular, analysis of multimodel simulations by *Aswathy et al*. [2015] report that both stratospheric aerosol injection and marine cloud brightening are able to decrease hot temperature extremes more than mean temperature, but provide limited mitigation potential for cold temperature extremes. This was also found in *Curry et al*. [2014], who examine the impact of solar reduction geoengineering on climate extremes in the GeoMIP G1 multimodel experiment, where warming of cold temperature extremes could not be avoided. This increase in minimum temperatures associated with stratospheric aerosol injection, marine cloud brightening, and solar reduction geoengineering in other studies is likely associated with the fact that these schemes are "active" during the daytime by reducing shortwave radiation and not reducing GHG concentrations. Similarly, in our experiments, we found some regional decrease of cool temperature extremes, particularly for low levels of crop albedo enhancement (e.g., Figures 4 and S5). Given that our single-model experiment finds similar warming of cold temperature extremes as multimodel experiments [e.g., *Curry et al*., 2014; *Aswathy et al*., 2015] it is perhaps an indication that most climate engineering is generally targeted at reducing hot extremes and not resolving all the challenges associated with future anthropogenic climate change. Therefore, although we only use a single model, we do find similarities between our results and those of previous studies. Resolving model

dependence can perhaps only be achieved by running coordinated CeLM experiments with several ESMs, which could involve the GeoMIP testbed [*Kravitz et al*., 2015].

5. Conclusions

Using idealized global simulations in an ESM, we have examined the potential of climate-effective land management (CeLM), consisting of crop albedo enhancement and irrigation, to reduce regional warming of hot extremes associated with future anthropogenic climate change. We note that the approach applied here is done globally while in reality the spatial extent may be less and therefore our results present the upper limit. We find that the considered CeLM implementations tend to be more effective at reducing hot temperature extremes by more than 2°C, while the effect on mean or cold temperature extremes is much less. We also find that implementing both irrigation and crop albedo enhancement is the most effective CeLM scheme that is examined here, which also has the potential to reduce water use from irrigation through decreases in evaporative demand. To our knowledge we are the first to demonstrate this potential. Furthermore, regional differences between irrigation and crop albedo enhancement were identified using a surface energy balance decomposition method. The regional differences were linked to how they respectively change the surface energy balance through changes in available energy and partitioning between Q_E and Q_H.

We find that a large albedo perturbation in our ESM is required to obtain a robust cooling response from crop albedo enhancement. This may present challenges on the feasibility of real-world implementation; however, our results are valid for globally applied scenarios. Other climate engineering schemes are known to have a significant termination effect. We find that over the winter months when CeLM is temporarily suspended, warming is possible due to persistent cloud cover that develops during the months when CeLM is active. Whether this is unique to the Community Earth System Model can only be confirmed by running similar experiments in other ESMs. Finally, the mitigation potential of CeLM is often underappreciated in the literature on idealized ESM experiments of climate engineering. However, our results demonstrate that perhaps this is due to the historical focus on examining how climate engineering will affect mean climate, where CeLM has limited influence, rather than the extremes where CeLM can have a substantial impact.

Acknowledgments

We thank National Center for Atmospheric Research (NCAR) for the development and access to the Community Earth System Model. We greatly thank the ETH Euler cluster for support with the computing resources of all climate model simulations. The authors would like to thank Urs Beyerle for providing the control ensemble simulations that were used as initial conditions of all idealized experiments. All authors acknowledge the European Research Council (ERC) "DROUGHT-HEAT" project funded by the European Community's Seventh Framework Programme (grant agreement FP7-IDEAS-ERC-617518). All materials that have contributed to the reported results are available upon request, including 10 TB of model output. All requests for data and analysis scripts should be directed to the corresponding authors A.L. Hirsch (annette.hirsch@env.ethz.ch) and S.I. Seneviratne (sonia.seneviratne@ethz.ch).

References

Aswathy, V. N., O. Boucher, M. Quaas, U. Niemeier, H. Muri, and J. Quaas (2015), Climate extremes in multi-model simulations of stratospheric aerosol and marine cloud brightening climate engineering, *Atmos. Chem. Phys.*, *15*, 9593–9610, doi:10.5194/acp-15-9593-2015.

Breuer, L., K. Eckhardt, and H. G. Frede (2003), Plant parameter values for models in temperate climates, *Ecol. Modell.*, *169*, 237–293, doi:10.1016/S0304-3800(03)00274-6.

Caldeira, K., and G. Bala (2016), Reflecting on 50 years of geoengineering research, *Earths Future*, *4*, 1–19, doi:10.1002/2016EF000454.

Cao, L., L. Duan, G. Bala, and K. Caldeira (2016), Simulated long-term climate response to idealized solar geoengineering, *Geophys. Res. Lett.*, *43*, 2209–2217, doi:10.1002/2016GL068079.

Crook, J. A., L. S. Jackson, S. M. Osprey, and P. M. Forster (2015), A comparison of temperature and precipitation responses to different Earth radiation management geoengineering schemes, *J. Geophys. Res. Atmos.*, *120*, 9352–9373, doi:10.1002/2015JD023269.

Crook, J. A., L. S. Jackson, and P. M. Forster (2016), Can increasing albedo of existing ship wakes reduce climate change?, *J. Geophys. Res. Atmos.*, *121*, 1545–1558, doi:10.1002/2015JD024201.

Crutzen, P. J. (2006), Albedo enhancement by stratospheric sulfur injections: A contribution to resolve a policy dilemma?, *Clim. Change*, *77*, 211–220, doi:10.1007/s10584-006-9101-y.

Curry, C. L., et al. (2014), A multi-model examination of climate extremes in an idealized geoengineering experiment, *J. Geophys. Res. Atmos.*, *119*, 3900–3923, doi:10.1002/2013JD020648.

Davin, E. L., S. I. Seneviratne, P. Ciais, A. Olioso, and T. Wang (2014), Preferential cooling of hot extremes from cropland albedo management, *Proc. Natl. Acad. Sci. U.S.A.*, *111*(27), 9757–9761, doi:10.1073/pnas.1317323111.

de Vrese, P., S. Hagemann, and M. Claussen (2016), Asian irrigation, African rain: Remote impacts of irrigation, *Geophys. Res. Lett.*, *43*, 3737–3745, doi:10.1002/2016GL068146.

Doughty, C. E., C. B. Field, and A. M. S. McMillan (2011), Can crop albedo be increased through the modification of leaf trichomes, and could this cool regional climate?, *Clim. Change*, *104*, 379–387, doi:10.1007/s10584-010-9936-0.

Drewry, D. T., P. Kumar, and S. P. Long (2014), Simultaneous improvement in productivity, water use, and albedo through crop structural modification, *Global Change Biol.*, *20*, 1955–1967, doi:10.1111/gcb.12567.

Febrero, A., S. Fernandez, J. L. Molina-Cano, and J. L. Araus (1998), Yield, carbon isotope discrimination, canopy reflectance and cuticular conductance of barley isolines of differing glaucousness, *J. Exp. Bot.*, *49*, 1575–1581, doi:10.1093/jxb/49.326.1575.

Feng, X., et al. (2016), Revegetation in China's Loess Plateau is approaching sustainable water resource limits, *Nat. Clim. Change*, *6*, 1019–1022, doi:10.1038/nclimate3092.

Fischer, E. M., U. Beyerle, and R. Knutti (2013), Robust spatially aggregated projections of climate extremes, *Nat. Clim. Change*, *3*(12), 1033–1038, doi:10.1038/nclimate2051.

Gabriel, C. J., A. Robock, L. Xia, B. Zambri, and B. Kravitz (2017), The G4Foam experiment: Global climate impacts of regional ocean albedo modification, *Atmos. Chem. Phys.*, *17*, 595–613, doi:10.5194/acp-17-595-2017.

Gent, P. R., et al. (2011), The community climate system model version 4, *J. Clim.*, *24*, 4973–4991, doi:10.1175/2011JCLI4083.1.
Glienke, S., P. J. Irvine, and M. G. Lawrence (2015), The impact of geoengineering on vegetation in experiment G1 of the GeoMIP, *J. Geophys. Res. Atmos.*, *120*, 10,196–10,213, doi:10.1002/2015JD024202.
Grant, R. H., G. M. Heisler, W. Gao, and M. Jenks (2003), Ultraviolet leaf reflectance of common urban trees and the prediction of reflectance from leaf characteristics, *Agric. For. Meteorol.*, *120*, 127–139, doi:10.1016/j.ag1formet.2003.08.025.
Hatfield, J. L., and R. E. Carlson (1979), Light quality distributions and spectral albedo of three maize canopies, *Agric. Meteorol.*, *20*, 215–226, doi:10.1016/0002-1571(79)90022-0.
Hurrell, J. W., et al. (2013), The community earth system model: A framework for collaborative research, *Bull. Am. Meteorol. Soc.*, *94*(9), 1339–1360, doi:10.1175/BAMS-D-12-00121.1.
Hurtt, G. C., S. Frolking, M. G. Fearon, B. Moore, E. Sheviliakova, S. Malyshev, S. W. Pacala, and R. A. Houghton (2006), The underpinnings of land-use history: Three centuries of global gridded land-use transitions, wood-harvest activity, and resulting secondary lands, *Global Change Biol.*, *12*, 1208–1229, doi:10.1111/j.1365-2486.2006.01150.x.
Intergovernmental Panel on Climate Change (IPCC) (2012), *Managing the Risks of Extreme Events and Disasters to Advance Climate Change Adaptation. A Special Report of Working Groups I and II of the Intergovernmental Panel on Climate Change*, edited by C. B. Field et al., 582 pp., Cambridge Univ. Press, Cambridge, U. K., and New York.
Intergovernmental Panel on Climate Change (IPCC) (2013), *Climate Change 2013: The Physical Science Basis. Contribution of Working Group I to the Fifth Assessment Report of the Intergovernmental Panel on Climate Change*, edited by T. F. Stocker et al., 1535 pp., Cambridge Univ. Press, Cambridge, U. K., and New York.
Irvine, P. J., A. Ridgwell, and D. J. Lunt (2010), Assessing the regional disparities in geoengineering impacts, *Geophys. Res. Lett.*, *37*, L18702, doi:10.1029/2010GL044447.
Irvine, P. J., A. Ridgwell, and D. J. Lunt (2011), Climatic effects of surface albedo geoengineering, *J. Geophys. Res.*, *116*, D24112, doi:10.1029/2011JD016281.
Irvine, P. J., B. Kravitz, M. G. Lawrence, and H. Muri (2016), An overview of the Earth system science of solar geoengineering, *WIREs Clim. Change*, 1–19, doi:10.1002/wcc.423.
Jones, A., J. Haywood, and O. Boucher (2009), Climate impacts of geoengineering marine stratocumulus clouds, *J. Geophys. Res.*, *114*, D10106, doi:10.1029/2008JD011450.
Jones, A., J. Haywood, O. Boucher, B. Kravitz, and A. Robock (2010), Geoengineering by stratospheric SO_2 injection: Results from the Met Office HadGEM2 climate model and comparison with the Goddard Institute for Space Studies ModelE, *Atmos. Chem. Phys.*, *10*, 5999–6006, doi:10.5194/acp-10-5999-2010.
Jones, A., et al. (2013), The impact of abrupt suspension of solar radiation management (termination effect) in experiment G2 of the Geoengineering Model Intercomparison Project (GeoMIP), *J. Geophys. Res. Atmos.*, *118*, 9743–9752, doi:10.1002/jgrd.50762.
Keith, D. (2000), Geoengineering the climate: History and prospect, *Annu. Rev. Energy Environ.*, *25*, 245–284.
Keith, D. W., and P. J. Irvine (2016), Solar geoengineering could substantially reduce climate risks—A research hypothesis for the next decade, *Earths Future*, 1–14, doi:10.1002/2016EF000465.
Kravitz, B., A. Robock, O. Boucher, H. Schmidt, K. E. Taylor, G. Stenchikov, and M. Schulz (2011), The Geoengineering Model Intercomparison Project (GeoMIP), *Atmos. Sci. Lett.*, *12*(2), 162–167, doi:10.1002/asl.316.
Kravitz, B., et al. (2013a), Climate model response from the Geoengineering Model Intercomparison Project (GeoMIP), *J. Geophys. Res. Atmos.*, *118*, 8320–8332, doi:10.1002/jgrd.50646.
Kravitz, B., et al. (2013b), An energetic perspective on hydrological cycle changes in the Geoengineering Model Intercomparison Project, *J. Geophys. Res. Atmos.*, *118*, 13,087–13,102, doi:10.1002/2013JD020502.
Kravitz, B., et al. (2015), The Geoengineering Model Intercomparison Project Phase 6 (GeoMIP6): Simulation design and preliminary results, *Geosci. Model Dev. Discuss.*, *8*, 4697–4736, doi:10.5194/gmd-8-3379-2015.
Kristjansson, J. E., H. Muri, and H. Schmidt (2015), The hydrological cycle response to cirrus cloud thinning, *Geophys. Res. Lett.*, *42*, 10,807–10,815, doi:10.1002/2015GL066795.
Lawrence, D. M., et al. (2011), Parameterization improvements and functional and structural advances in Version 4 of the Community Land Model, *J. Adv. Model. Earth Syst.*, *3*, M03001, doi:10.1029/2011MS000045.
Lenton, T. M., and N. E. Vaughan (2009), The radiative forcing potential of different climate geoengineering options, *Atmos. Chem. Phys.*, *9*, 5539–5561, doi:10.5194/acp-9-5539-2009.
Lobell, D. B., G. Bala, and P. B. Duffy (2006), Biogeophysical impacts of cropland management changes on climate, *Geophys. Res. Lett.*, *33*, L06708, doi:10.1029/2005GL025492.
Luyssaert, S., et al. (2014), Land management and land-cover change have impacts of similar magnitude on surface temperature, *Nat. Clim. Change*, *4*(5), 389–393, doi:10.1038/nclimate2196.
Meehl, G. A., et al. (2013), Climate change projections in CESM1 (CAM5) compared to CCSM4, *J. Clim.*, *26*(17), 6287–6308, doi:10.1175/JCLI-D-12-00572.1.
Muri, H., U. Niemeier, and J. E. Kristjansson (2015), Tropical rainforest response to marine sky brightening climate engineering, *Geophys. Res. Lett.*, *42*, 2951–2960, doi:10.1002/2015GL063363.
Neale, R. B., et al. (2012), Description of the NCAR Community Atmosphere Model (CAM 5.0), NCAR Tech. Note TN-486, 274 pp.
Niemeier, U., H. Schmidt, K. Alterskjaer, and J. E. Kristjánsson (2013), Solar irradiance reduction via climate engineering: Impact of different techniques on the energy balance and the hydrological cycle, *J. Geophys. Res. Atmos.*, *118*, 11, 905–11, 917, doi:10.1002/2013JD020445.
Oleson, K., et al. (2013), Technical description of version 4.5 of the Community Land Model (CLM) (No. TN-503+STR), pp. 1–434, National Center for Atmospheric Research, Boulder, Colo.
Oleson, K. W., et al. (2010), Technical description of version 4.0 of the Community Land Model (CLM) (No. NCAR/TN-478+STR), pp. 1–266, National Center for Atmospheric Research, Boulder, Colo.
Perkins, S. E., and E. M. Fischer (2013), The usefulness of different realizations for the model evaluation of regional trends in heat waves, *Geophys. Res. Lett.*, *40*, 5793–5797, doi:10.1002/2013GL057833.
Piggin, I., and P. Schwerdtfeger (1973), Variations in the albedo of wheat and barley crops, *Archive Meteorol. Geophys. Bioclimatol.*, *21*, 365–391, doi:10.1007/BF02253314.
Pittelkow, C. M., et al. (2015), Productivity limits and potentials of the principles of conservation agriculture, *Nature*, *517*, 365–368, doi:10.1038/nature13809.
Riahi, K., et al. (2011), RCP 8.5—A scenario of comparatively high greenhouse gas emissions, *Clim. Change*, *109*(1–2), 33–57, doi:10.1007/s10584-011-0149-y.

Ridgwell, A., J. S. Singarayer, A. M. Hetherington, and P. J. Valdes (2009), Tackling regional climate change by leaf albedo bio-geoengineering, *Curr. Biol.*, *19*(2), 146–150, doi:10.1016/j.cub.2008.12.025.

Robock, A., L. Oman, and G. Stenchikov (2008), Regional climate responses to geoengineering with tropical and Arctic SO_2 injections, *J. Geophys. Res.*, *113*, D16101, doi:10.1029/2008JD010050.

Sacks, W. J., B. I. Cook, N. Buenning, S. Levis, and J. H. Helkowski (2009), Effects of global irrigation on the near-surface climate, *Clim. Dyn.*, *33*, 159–175, doi:10.1007/s00382-008-0445-z.

Schaller, N., J. Sadlácek, and R. Knutti (2014), The asymmetry of the climate system's response to solar forcing changes and its implications for geoengineering scenarios, *J. Geophys. Res. Atmos.*, *119*, 5171–5184, doi:10.1002/2013JD021258.

Seneviratne, S. I., T. Corti, E. L. Davin, M. Hirschi, E. B. Jaeger, I. Lehner, B. Orlowsky, and A. J. Teuling (2010), Investigating soil moisture-climate interactions in a changing climate: A review, *Earth Sci. Rev.*, *99*, 125–161, doi:10.1016/j.earscirev.2010.02.004.

Seneviratne, S. I., et al. (2012), Changes in climate extremes and their impacts on the natural physical environment, in *Managing the Risks of Extreme Events and Disasters to Advance Climate Change Adaptation*, A Special Report of Working Groups I and II of the Intergovernmental Panel on Climate Change (IPCC), edited by C. B. Field et al., pp. 109–230, Cambridge Univ. Press, Cambridge, U. K., and New York.

Seneviratne, S. I., M. G. Donat, A. J. Pitman, R. Knutti, and R. L. Wilby (2016), Allowable CO_2 emissions based on regional and impact-related climate targets, *Nature*, *529*, 477–483, doi:10.1038/nature16542.

Singarayer, J. S., A. Ridgwell, and P. Irvine (2009), Assessing the benefits of crop albedo bio-geoengineering, *Environ. Res. Lett.*, *4*, 045110, doi:10.1088/1748-9326/4/4/045110.

Sonntag, S., J. Pongratz, C. H. Reick, and H. Schmidt (2016), Reforestation in a high-CO2 world—Higher mitigation potential than expected, lower adaptation potential than hoped for, *Geophys. Res. Lett.*, *43*, 1–8, doi:10.1002/2016GL068824.

Thiery, W., E. L. Davin, D. M. Lawrence, A. L. Hirsch, M. Hauser, and S. I. Seneviratne (2017), Present-day irrigation mitigates heat extremes, *J. Geophys. Res. Atmos.*, doi:10.1002/2016JD025740.

Thornton, P. E., J.-F. Lamarque, N. A. Rosenbloom, and N. M. Mahowald (2007), Influence of carbon-nitrogen cycle coupling on land model response to CO_2 fertilization and climate variability, *Global Biogeochem. Cycles*, *21*, GB4018, doi:10.1029/2006GB002868.

Tilmes, S., et al. (2013), The hydrological impact of geoengineering in the Geoengineering Model Intercomparison Project (GeoMIP), *J. Geophys. Res. Atmos.*, *118*, 11,036–11,058, doi:10.1002/jgrd.50868.

Tjiputra, J. F., A. Grini, and H. Lee (2016), Impact of idealized future stratospheric aerosol injection on the large-scale ocean and land carbon cycles, *J. Geophys. Res. Biogeosci.*, *120*, 2–27, doi:10.1002/2015JG003045.

Uddin, M. N., and D. R. Marshall (1988), Variation in epicuticular wax content in wheat, *Euphytica*, *38*, 3–9, doi:10.1007/BF00024805.

United Nations Framework Convention on Climate Change (2015), Adoption of the Paris Agreement. Report No. FCCC/CP/2015/L.9/Rev.1. [Available at http://unfccc.int/resource/docs/2015/cop21/eng/l09r01.pdf.]

van Dijk, A. I. J. M., et al. (2013), The millennium drought in southeast Australia (2001–2009): Natural and human causes and implications for water resources, ecosystems, economy, and society, *Water Resour. Res.*, *49*, 1040–1057, doi:10.1002/wrcr.20123.

Vaughan, N. E., and T. M. Lenton (2011), A review of climate geoengineering proposals, *Clim. Change*, *109*, 745–790, doi:10.1007/s10584-011-0027-7.

Wigley, T. M. L. (2006), A combined mitigation/geoengineering approach to climate stabilization, *Science*, *314*, 452–454, doi:10.1126/science.1131728.

Wilhelm, M., E. L. Davin, and S. I. Seneviratne (2015), Climate engineering of vegetated land for hot extremes mitigation: An Earth system model sensitivity study, *J. Geophys. Res. Atmos.*, *120*, 2612–2623, doi:10.1002/2014JD022293.

Xia, L., A. Robock, S. Tilmes, and R. R. Neely (2016), Stratospheric sulfate geoengineering could enhance the terrestrial photosynthesis rate, *Atmos. Chem. Phys.*, *16*, 1479–1489, doi:10.5194/acp-16-1479-2016.

Zamft, B. M., and R. J. Conrado (2015), Engineering plants to reflect light: Strategies for engineering water-efficient plants to adapt to a changing climate, *Plant Biotechnol. J.*, *13*, 867–874, doi:10.1111/pbi.12382.

Zhang, X., L. Alexander, G. C. Hegerl, P. Jones, A. Klein Tank, T. C. Peterson, B. Trewin, and F. W. Zwiers (2011), Indices for monitoring changes in extremes based on daily temperature and precipitation data, *Wiley Interdiscip. Rev. Clim. Change*, *2*, 851–870, doi:10.1002/wcc.147.